4.0 PROBABILISTIC VOLCANIC HAZARD ANALYSIS RESULTS

This section presents the results of the probabilistic volcanic hazard analysis (PVHA) performed using the hazard models developed by the 10 experts. The results are presented first for the individual experts in Section 4.1. Section 4.2 presents the aggregated result.

4.1 RESULTS FOR INDIVIDUAL EXPERT PVHA MODELS

Section 3.2 presents the 10 PVHA models developed for this study. Each model is presented in the form of a logic tree (Figures 3-15 and 3-16) that explicitly incorporates the uncertainty in selecting appropriate probabilistic models and model parameters to describe the spatial and temporal occurrence of future volcanic events in the vicinity of the proposed Yucca Mountain repository site and to describe the geometry (length and azimuth) of basaltic dikes associated with these events. Each end branch of these logic trees defines a possible set of models and model parameters that provide an estimate of the annual frequency of intersection of the repository footprint by a volcanic event. The associated probability of the end branch (obtained by multiplying all of the conditional probabilities along the path to the end branch) represents the likelihood that the computed frequency of intersection is the "correct" value for the site volcanic hazard. Thus, the computed results for all of the end branches and their associated probabilities define a probability distribution for the annual frequency of intersection.

The PVHA computation consisted of calculating the rate density of volcanic events on a 1-km by 1-km grid throughout the region defined by the local source zones. Similarly, the conditional probability of intersection was computed for the same grid of points. At each point in the grid the rate density of events was multiplied by the conditional probability of intersection, and the result summed over all points in the grid to yield the annual frequency of intersection.

The computation process was repeated for all possible combinations of event geometries, temporal models, time periods, spatial models, source zone definitions, smoothing parameters, event counts, and statistical distributions in rate estimates defined by the logic tree developed for each expert. The discrete distributions were used to compute the expected frequency of intersection and statistics of the uncertainty in the frequency of intersection. The results for the individual experts are presented below in alphabetical order by first initial.

Alexander McBirney Figure 4-1 presents the results of the hazard computation performed using the PVHA model developed by Alexander McBirney (AM). Part (a) of Figure 4-1 shows a histogram representation of the discrete density distribution for annual frequency of intersection. The histogram uses equal interval widths on a log scale. The mean of the distribution and the 5th-, 50th- (median), and 95th -percentiles of the distribution are indicated on the plot. The mean frequency of intersection is $4.3 \cdot 10^{-9}$ and the 90-percent confidence interval (5th- to 95th-percentile) ranges from $6.9 \cdot 10^{-10}$ to $1.8 \cdot 10^{-8}$. The distribution is skewed to the right, indicating that the preferred models and parameters lead to lower hazard than the mean.

The distribution for frequency of intersection shown on part (a) of Figure 4-1 results from uncertainties in a number of components of the PVHA hazard model. Part (b) of Figure 4-1 presents in summary form the relative contribution of the uncertainty in each of the PVHA components to the total uncertainty in the computed hazard. The plot is in the form of a histogram showing the percent of the total variance in the frequency of intersection that is due to uncertainty in the individual model components specified by Alexander McBirney. The parameters are arranged in the order that they appear in the general PVHA model logic tree (Figures 3-15 and 3-16).

In the PVHA model developed by Alexander McBirney approximately 50 percent of the total variance is due to uncertainty in the spatial model. The next largest contributor to the uncertainty in the hazard is the uncertainty in the rate parameter. As discussed in Section 3.1, the statistical uncertainty in computing the rate of volcanic events from a small data set was included as part of the uncertainty in the PVHA model. The results shown on part (b) of Figure 4-1 indicate that the uncertainty in estimating the rate from a small sample is a significant portion of the total uncertainty. The uncertainty in the hazard resulting from the combined uncertainty in defining the number of events at all of the volcanic centers is the next largest contributor. The impact of uncertainty in the counts at Buckboard Mesa is larger because the events at this center are the basis for the event rates in three source zones, including the one in which the repository is located (Zone-4).

The plot on part (b) of Figure 4-1 list all 24 components of the overall PVHA model defined on Figures 3-15 and 3-16. Many components have no contribution to the variance in the hazard computed by Alexander McBirney's PVHA model because they were not modeled as uncertain. These components are marked by a * on the figure.

Figure 4-2 shows the effect of the choice of maximum dike length and time period on the hazard. These distributions are conditional on the specified parameter. For example, the distribution for a maximum dike length of 15 km was computed by assigning a probability of 1.0 to this maximum dike length in the Alexander McBirney's PVHA model logic tree and probability zero to all other maximum dike lengths. The potential for longer dikes leads to slightly higher hazard estimates. Use of only the post-1 Ma time period leads to higher hazard than computed for the post-5 Ma time period because of the resulting higher frequency for events within the region of interest.

Figure 4-3 shows the effect of the choice of spatial model and the choice of smoothing parameter, h, on the computed hazard. Use of the kernel smoothing approach leads to significantly higher hazard because it allows for the relatively higher rate of events in Crater Flat to diffuse outward, and thus increase the rate density of events in the vicinity of the repository. The results for the different values of h are presented conditional on the use of the kernel smoothing approach. The increase in h from 6 km to 12 km has only a minor effect on the computed hazard. Connor and Hill (1995) also found relatively small differences in the hazard (less than a factor of 2) for comparable changes in h.

Bruce Crowe Figure 4-4 presents the results of the hazard computation performed using the PVHA model developed by Bruce Crowe (BC). The mean frequency of intersection is $1.1 \cdot 10^{-8}$ and the 90-percent confidence interval (5^{th}- to 95^{th}-percentile) ranges from $7.4 \cdot 10^{-10}$ to $3.5 \cdot 10^{-8}$. Part (b) of Figure 4-4 presents the relative contribution of the uncertainty in each of the PVHA components to the total uncertainty in the computed hazard. The largest contributor to uncertainty is the choice of time period. The second largest contributor is the uncertainty in zonation. The uncertainty in zonation is conditional on a selected time period and zonation model. For example, it reflects the choice between the alternative zones defined for the Quaternary time period and the structural approach to zonation. The large impact of the uncertainty in zonation on the hazard results arises from alternatives that sometimes place the repository site in zones with high event counts. The next largest contributor to the uncertainty in the hazard is, again, the uncertainty in the rate parameter estimated from a limited data set. Uncertainties in defining the region of interest and in defining the event counts within these regions also have significant contributions to the total uncertainties. Many of the zonation models defined by Bruce Crowe have source zones that do not include the site, and the site hazard is due primarily to the rate density of events in the background zone.

Figure 4-5 shows the effect of the choice of dike length distribution and temporal model on the hazard. The Gaussian dike length distribution has the potential for longer dikes, leading to slightly higher hazard estimates. The homogeneous temporal model results in slightly higher hazard estimates than the nonhomogeneous model because the average β values computed for the Weibull process are less than 1.

Figure 4-6 shows the effect of the choice of time period on the computed hazard. The use of the Plio-Quaternary time period produces significantly higher hazard estimates because the zonation models developed for this time period place higher weight on source zones that include both the site and the events in Crater Flat. The different peaks of the conditional distributions for the Quaternary and Plio-Quaternary time periods produce the bimodal combined distribution shown on part (a) of Figure 4-4. The distribution for the Mio-Plio-Quaternary time period is much narrower than for the other time periods because there are no alternative zonations and the uncertainty in the event rates are smaller because of the larger data sets used to make the estimates.

George Thompson Figure 4-7 presents the results of the hazard computation performed using the PVHA model developed by George Thompson (GT). The mean frequency of intersection is $3.3 \cdot 10^{-8}$ and the 90-percent confidence interval (5^{th}- to 95^{th}-percentile) ranges from $7.2 \cdot 10^{-9}$ to $7.4 \cdot 10^{-8}$. Part (b) of Figure 4-7 presents the relative contribution of the uncertainty in each of the PVHA components to the total uncertainty in the computed hazard. The largest contributor to uncertainty is the uncertainty in the rate parameter estimated from a limited data set. Uncertainty in the amount of hidden events (either none or equal to the number of observed events) also is a large contributor to the total uncertainty because it has a significant impact on the overall rate of events.

Figure 4-8 shows the effect of the choice of maximum dike length and time period on the hazard. The alternative maximum dike lengths are similar and produce nearly identical hazard results. Use of the post-1 Ma time period results in higher hazard because of the forecasted higher event frequencies.

George Walker Figure 4-9 presents the results of the hazard computation performed using the PVHA model developed by George Walker (GW). The mean frequency of intersection is $5.8 \cdot 10^{-9}$ and the 90-percent confidence interval (5^{th}- to 95^{th}-percentile) ranges from $9.7 \cdot 10^{-10}$ to $1.5 \cdot 10^{-8}$. Part (b) of Figure 4-9 presents the relative contribution of the uncertainty in each of the PVHA components to the total uncertainty in the computed hazard. The largest contributor to uncertainty

is the uncertainty in the rate parameter estimated from a limited data set. Uncertainty in the amount of hidden events (ranging from none to four times the number of observed events) is the second largest contributor because of the large impact on the overall rate of events. The uncertainty in the Gaussian field parameters also has a large contribution to the total uncertainty because they affect the rate density of events near the site associated with the Crater Flat Volcanic Zone.

Figure 4-10 shows the effect of the choice of maximum dike length and spatial model on the hazard. The alternative maximum dike lengths have a significant impact on the hazard because longer dike lengths allow for a greater contribution from events occurring in the Crater Flat Volcanic Zone. The Gaussian field shape and kernel smoothing spatial models produce higher hazard than the zonation model because they allow for the higher rate density of events in Crater Flat to diffuse outward towards the site.

Mel Kuntz. Figure 4-11 presents the results of the hazard computation performed using the PVHA model developed by Mel Kuntz (MK). The mean frequency of intersection is $9.9 \cdot 10^{-9}$ and the 90-percent confidence interval (5^{th}- to 95^{th}-percentile) ranges from $3.2 \cdot 10^{-10}$ to $3.1 \cdot 10^{-8}$. Part (b) of Figure 4-11 presents the relative contribution of the uncertainty in each of the PVHA components to the total uncertainty in the computed hazard. The largest contributor to uncertainty is the uncertainty in the rate parameter estimated from a limited data set. The other major contributor to the uncertainty in the hazard is the uncertainty in the spatial model. Uncertainty in the smoothing parameter, h, the Gaussian field parameters, and the form of the transition across local zone boundaries (abrupt versus gradual) all have minor contributions to the total uncertainty.

Figure 4-12 shows the effect of the choice of maximum dike length on the hazard. The alternative maximum dike lengths have a smaller impact on the hazard than was the case for George Walker's PVHA model because in Mel Kuntz's PVHA model the background source has a rate density closer to that of Crater Flat and, as a result, a larger contribution to the total hazard. The large change in maximum dike length from 10 to 18 km results in only a small change in the distribution for frequency of intersection, primarily in raising the lower tail. Most of the hazard in Mel Kuntz's PVHA model comes from events occurring near the proposed repository site, either in the local source zone, or from the Crater Flat zone when using the kernel smoothing or Gaussian field spatial models because most of the probability density for dike length is placed on short lengths (<5 km). Changes in maximum dike length produce only small changes in the bulk

of the dike length distribution, and thus lead to small changes in the conditional probability of intersection.

Figure 4-13 shows the effect of the choice of temporal model and time period on the hazard. The nonhomogeneous temporal model results in slightly higher hazard estimates than the homogeneous model because the average β values computed for the Weibull process using Mel Kuntz's assessments of the appropriate time periods are greater than 1. As was the case for the results of other experts discussed above, the use of the post-2 Ma time period results in higher hazard than that obtained with longer time periods.

Figure 4-14 shows the effect of the choice of spatial model on the hazard. The uniform model produces the highest hazard because it results in the highest event rate density in the repository vicinity. The zonation model produces the lowest event rate density in the site vicinity, and thus the lowest hazard.

Michael Sheridan Figure 4-15 presents the results of the hazard computation performed using the PVHA model developed by Michael Sheridan (MS). The mean frequency of intersection is $1.8 \cdot 10^{-8}$ and the 90-percent confidence interval (5 th- to 95 th-percentile) ranges from $2.9 \cdot 10^{-9}$ to $4.7 \cdot 10^{-8}$. Part (b) of Figure 4-15 presents the relative contribution of the uncertainty in each of the PVHA components to the total uncertainty in the computed hazard. The largest contributor to uncertainty is the uncertainty in the rate parameter estimated from a limited data set. Other significant contributors to the uncertainty in the hazard are the uncertainty in dike length distribution, spatial model, and Gaussian field parameters. Michael Sheridan's PVHA model includes the possibility that the Lathrop Wells event has not ended and a future eruption associated with this event may occur. The uncertainty whether or not the Lathrop Wells event has ended is represented on part (b) of Figure 4-15 by the uncertainty in zonation model (whether or not to include Lathrop Wells as an additional source zone). This uncertainty also contributes significantly to the total uncertainty.

Figures 4-16 and 4-17 show the effect of the choice of dike length distribution on the hazard. Those distributions that result in longer dike lengths produce higher hazard because they allow for greater contribution from the Crater Flat field and from the Lathrop Wells event (when it is assumed to be still active).

Figure 4-18 shows the effect of the choice of spatial model and the uncertainty in the termination of the Lathrop Wells event on the hazard. The uniform model produces higher hazard than the Gaussian field model because it results in higher event rate density in the repository vicinity. The potential for continuation of the Lathrop Wells event results in higher hazard because of the associated high frequency of an additional dike emplacement (10^{-5} per year).

Richard Carlson Figure 4-19 presents the results of the hazard computation performed using the PVHA model developed by Richard Carlson (RC). The mean frequency of intersection is $1.4 \cdot 10^{-8}$ and the 90-percent confidence interval (5^{th}- to 95^{th}-percentile) ranges from $1.0 \cdot 10^{-9}$ to $4.5 \cdot 10^{-8}$. Part (b) of Figure 4-19 presents the relative contribution of the uncertainty in each of the PVHA components to the total uncertainty in the computed hazard. The largest contributor to uncertainty is the uncertainty in the rate parameter estimated from a limited data set. The other significant contributors to the uncertainty in the hazard are the uncertainty in the spatial model, uncertainty in the smoothing parameter, h, and uncertainty in the counts at northwestern Crater Flat (NWCF). Uncertainty in event counts affects the spatial distribution of events used to perform the kernel smoothing as well as the overall rate of events. In particular, the spatial extent of the events at northwestern Crater Flat impacts the computation of the spatial density in the site vicinity.

Figure 4-20 shows the effect of the choice of maximum dike length on the hazard for the random. The alternative maximum dike lengths have a small impact on the hazard.

Figure 4-21 shows the effect of the choice of temporal and spatial models on the hazard. The nonhomogeneous temporal model results in slightly lower hazard estimates than the homogeneous model because, although it predicts a higher overall rate of events, the events are more spatially diffuse, resulting in a lower predicted spatial density in the repository vicinity. The uniform model produces higher hazard than the kernel smoothing model because it results in higher event rate density in the repository vicinity.

Richard Fisher Figure 4-22 presents the results of the hazard computation performed using the PVHA model developed by Richard Fisher (RF). The mean frequency of intersection is $1.8 \cdot 10^{-8}$ and the 90-percent confidence interval (5^{th}- to 95^{th}-percentile) ranges from $3.4 \cdot 10^{-9}$ to $4.1 \cdot 10^{-8}$. Part (b) of Figure 4-22 presents the relative contribution of the uncertainty in each of the PVHA components to the total uncertainty in the computed hazard. The largest contributor to uncertainty is the uncertainty in the rate parameter estimated from a limited data set. The next largest contributor is the uncertainty in the event counts within the regions of interest (other zone event

counts). Other significant contributors to the uncertainty in the hazard are the uncertainty in the time period, region of interest, spatial model, and the event counts for northwestern Crater Flat.

Figure 4-23 shows the effect of the choice of maximum dike length and time period on the hazard. The alternative maximum dike lengths have a small impact on the hazard. The alternative time periods of post-1 Ma and post-2 Ma produce estimates of the hazard that are different by approximately a factor of two because there is little difference in the event counts within these two time periods.

Figure 4-24 shows the effect of the choice of region of interest and spatial model on the hazard. The use of the eastern zone as the region of interest produces higher hazard because it includes two additional areas with large event counts (Lunar Crater and Cima), resulting in a higher rate density within the background zone. The zonation model produces the lowest hazard and the kernel smoothing model produces the highest hazard because of the relative difference in the spatial density in the site vicinity. The Gaussian field model produce similar estimates of the hazard to that obtained from the zonation model because Richard Fisher restricted the field parameters and the kernel smoothing parameter to produce the same spatial density contours at the boundary of the Crater Flat zone.

Wendell Duffield. Figure 4-25 presents the results of the hazard computation performed using the PVHA model developed by Wendell Duffield (WD). The mean frequency of intersection is $1.6 \cdot 10^{-9}$ and the 90-percent confidence interval (5^{th}- to 95^{th}-percentile) ranges from $8.7 \cdot 10^{-11}$ to $4.3 \cdot 10^{-9}$. Part (b) of Figure 4-25 presents the relative contribution of the uncertainty in each of the PVHA components to the total uncertainty in the computed hazard. The largest contributor to uncertainty is the uncertainty in the rate parameter estimated from a limited data set. The other significant contributors to the uncertainty in the hazard are the uncertainty in the maximum dike length and the uncertainty in the potential for a hidden event in the background zone, which is included as uncertainty in other event counts.

Figure 4-26 shows the effect of the choice of maximum dike length and zonation model on the hazard. Consideration of longer maximum dike lengths leads to significantly higher hazard estimates. Wendell Duffield's spatial model is a source zone encompassing Crater Flat and a background zone in the vicinity of the site with a substantially lower rate density of volcanic events. Thus, most of the hazard is associated with events in the Crater Flat zone and increasing the maximum dike length leads to a higher likelihood that events occurring in the Crater Flat

source zone will intersect the repository. Use of the alternative representations for Zone B and C_{WL} leads to the same hazard because it does not impact the event rate density in the site vicinity.

William Hackett Figure 4-27 presents the results of the hazard computation performed using the PVHA model developed by William Hackett (WH). The mean frequency of intersection is $3.0 \cdot 10^{-8}$ and the 90-percent confidence interval (5^{th}- to 95^{th}-percentile) ranges from $5.6 \cdot 10^{-9}$ to $7.8 \cdot 10^{-8}$. Part (b) of Figure 4-27 presents the relative contribution of the uncertainty in each of the PVHA components to the total uncertainty in the computed hazard. The largest contributor to uncertainty is the uncertainty in the spatial model. Uncertainty in the rate parameter and uncertainty in the smoothing parameter, *h*, result in similar levels of uncertainty in the hazard.

Figure 4-28 shows the effect of the choice of maximum dike length on the hazard. The alternative maximum dike lengths produce only small differences in the hazard because most of the hazard results from near by events.

Figure 4-29 shows the effect of the uncertainty in mean dike azimuth on the computed hazard. There is a gradual increase in the hazard as the mean azimuth changes from N05°E to N45°E. This increase results from a greater number of dikes associated with potential future events being oriented towards the repository site in the post-1 Ma source zone.

Figure 4-30 shows the effect of the choice of time period and spatial model on the hazard. The highest hazard results from use of the post-5 Ma time period. The post-1 Ma and post-5 Ma time periods have similar estimates of the rate of events in the region of interest, but the repository site lies within the source zone for the post-5 Ma time period. The zonation model produces lower hazard than the kernel smoothing model because the favored zonation (the post-1 Ma zone) does not include the site in the zone with the highest event rate.

4.2 AGGREGATE HAZARD

Figure 4-31 compares the hazard results obtained for the 10 PVHA models developed by the volcanic experts. The relative smoothness of the distributions reflects the number of discrete end branches of the logic trees defined by each expert. However, all of the distributions span a large range in the estimates of the frequency of intersection, indicating that each expert considered that there are significant uncertainties in estimating the hazard.

Computing the aggregate distribution for the frequency of intersection requires specification of the weight to be assigned to each expert's distribution. As stated in Section 2.2.11, the objective from the beginning of the study was to be able to apply equal weights to the experts' assessments of the volcanic hazard. For the reasons given in Section 2.2.11, it is our judgment that this objective has been achieved and equal weights are appropriate.

Figure 4-32 shows the aggregate hazard results. Part (a) shows the aggregate of the 10 distributions shown on Figure 4-31. The mean frequency of intersection is $1.5 \cdot 10^{-8}$ and the 90-percent confidence interval (5^{th}- to 95^{th}-percentile) ranges from $5.4 \cdot 10^{-10}$ to $4.9 \cdot 10^{-8}$. Also shown on the plot are the mean and median values for the 10 individual experts' distributions. The individual means and medians span about one and one-half orders of magnitude and all lie within the 90-percent confidence interval of the aggregate distribution. The aggregate distribution is skewed somewhat to the left (in log space), with a concentration of mass near the mean frequency of intersection. The distributions of the individual medians and means mirror this general shape.

Part (b) of Figure 4-32 compares the 90-percent confidence intervals computed for the 10 individual experts' distributions to the 90-percent confidence interval for the aggregate distribution. The medians and means from part (a) are also shown. Nearly all of the individual confidence intervals overlap each other and all but one of the individual confidence intervals contain the aggregate median and mean. The lowest hazard estimates result from Wendell Duffield's model in which very strong preference is placed on the most recent past for predicting the future and on restricting events to Crater Flat. The median and mean values computed from his PVHA model lie within most of the individual 90-percent confidence intervals.

Figure 4-33 presents the relative contribution of the uncertainty in each of the PVHA components to the total uncertainty in the aggregate hazard. Part (a) shows the total variance split into inter-expert (expert to expert differences) and intra-expert (individual expert uncertainty) components. The expert-to-expert differences represent about one-third of the total variance in the frequency of intersection. The majority of the uncertainty in the hazard results from the uncertainties specified by the individual experts (intra-expert uncertainty).

Part (b) of Figure 4-33 shows the breakdown of the intra-expert variance among the various components of the PVHA model logic tree. This plot shows the relative contribution to the total intra-expert variance averaged over all experts. The largest component of the intra-expert uncertainty results from the statistical uncertainty in estimating the event rates. This component

(approximately 40 percent of the intra-expert variance) is significantly larger than the combined contributions of uncertainties in evaluating the event counts at the various volcanic centers (approximately 11 percent of the intra-expert variance). The second largest component of the intra-expert uncertainty in the hazard results from uncertainty in the appropriate spatial model (approximately 14 percent of the intra-expert variance). Uncertainty in defining the parameters of the various spatial models together contribute a comparable level of uncertainty (approximately 13 percent of the intra-expert variance). The modeled uncertainty in the temporal models and appropriate time period have a smaller contribution to the total uncertainty, as does uncertainty in the dike length distributions.

Figures 4-34 through 4-37 show various sensitivity analysis results. Figure 4-34 shows the effect of the choice of maximum dike length and temporal model on the aggregate hazard distribution for frequency of intersection. Conditional distributions were computed using only each experts minimum value for maximum dike length and each experts maximum value for maximum dike length. The range in maximum dike lengths produces only a small change in the hazard (approximately 30 percent difference in the mean frequency of intersection). This small effect is because the experts placed most of the probability mass on short lengths in their dike length distributions. Thus, the effect of alternative maximum dike lengths was to change the conditional probability of intersection function (e.g Figure 3-14) only in the area where the conditional probability is very low. At the same time, nearly all of the experts' assessments contained spatial models that produced event densities in the vicinity of the proposed repository site that are a significant fraction of those estimated for Crater Flat. As a result, the majority of the hazard results from the potential occurrence of events near the repository and is relatively insensitive to the assigned maximum dike length.

Use of the homogeneous and nonhomogeneous temporal models produces very similar estimates of the volcanic hazard. (Note that only three of the experts, BC, MK, and RC, included nonhomogeneous temporal models in their assessments and the results shown on Figure 4-34 for the nonhomogeneous model are the aggregate of these three conditional distributions.)

Figure 4-35 shows the effect of the choice of time period on the aggregate hazard distribution. Conditional results are shown for the Quaternary period (post 1 or 2 Ma), the Plio-Quaternary period (post ~5 Ma), and the Mio-Plio-Quaternary period (post ~10 Ma). (Again note that the results are the aggregate of the conditional distributions for those experts that included the particular time period as an alternative in their PVHA model.) Use of the Quaternary and Plio-

Quaternary time period produces similar hazard estimates and the results for the post-10 Ma time period are slightly lower. The conditional distribution for the Quaternary time period is broader in part because the event occurrence rates are estimated from fewer numbers of events and are thus more uncertain.

Figure 4-36 shows the effect of the choice of spatial model on the aggregate hazard distribution. Use of the uniform model produces the highest hazard because the site always lies in this source zone. The zonation models produce the lowest hazard because they typically restrict the highest rate density of events to Crater Flat. The zonation models also produce the broadest conditional distribution because the alternative source zones result in substantial changes in the event rate density estimates in the site vicinity. However, all of the conditional mean estimates of the frequency of intersection for the four spatial models are within a factor of two of each other.

All of the hazard estimates presented above were computed using the randomly placed dike representation of volcanic events [part (c) of Figure 3-11]. As a sensitivity analysis, the frequency of intersection was also computed using the two other event representations discussed in Section 3, point events and dikes centered on the event (see Figure 3-11). Point events were considered to have intersected the repository if they occurred within 0.25 km of the repository boundary. Figure 4-37 compares the resulting aggregate distributions for frequency of intersection. The mean values for frequency of intersection are $5.7 \cdot 10^{-9}$, $1.4 \cdot 10^{-8}$, and $1.5 \cdot 10^{-8}$ for point events, event-centered dikes, and random dikes, respectively. Note that the distribution computed for the point representation of events has significant probability mass at annual frequencies lower than 10^{-12} and the 5th-percentile is plotted at 10^{-12} on the figure. The event-centered dike and the random dike representations of events produce very similar estimates of hazard for the same reason that the aggregate results are relatively insensitive to the assessment of the maximum dike length.

Finally, we examined the sensitivity of the results to expert selection. The results shown on Figure 4-32 are the aggregate assessments of 10 individuals selected from the available population of experts on basaltic volcanism. One may ask what would have been the result if a different group of equally qualified experts had been selected and subjected to the same process. Also, one may ask what is the sensitivity of the answer to the size of the panel selected. Two analyses were performed to examine this issues.

First, it is possible to examine the range of results for subsets of the expert panel. For example, there are 10 possible subsets of 9 experts, 252 possible subsets of 5 experts, and 10 possible subsets of 1 expert. For each subset, an aggregate distribution for the frequency of intersection can be computed, and the resulting mean hazard and percentiles of the hazard distribution obtained. The range in the various statistics is a possible indication of the range one might obtain from other expert panels of smaller size.

Figure 4-38 presents the results of this type of analysis. All possible subsets of from 1 to 10 experts were defined and an aggregate distribution for frequency of intersection computed for each subset. The resulting range in mean values and the 5th and 95th percentiles of the combined distributions are plotted as continuous curves on the figure versus the number of experts in the subsets. The results indicate that for subsets of greater than five experts, the range in mean hazard and in the 95th percentile hazard are relatively small. The 5th percentile of the hazard distribution shows more variability among the experts than the other two measures. This is because the lower hazard estimates are more sensitive to the details of the hazard models (placement of zone boundaries, dike length distributions) than are the mean and 95th percentile hazard estimates. The results for the 95th percentile hazard are somewhat limited by the maximum event frequencies one can estimate from the observed data, and thus do to vary greatly among the experts.

A second approach to evaluating the variability in the hazard estimates is to use the bootstrapping technique. Assuming that the selected panel is representative of the population of qualified experts, then one can simulate a new panel of 10 experts by randomly selecting experts from the existing panel. The selection is done with replacement (i.e an expert can be selected more than once) because it is assumed that each expert is equally likely to represent a member of the population of qualified experts. The aggregate distribution computed from the simulated expert panel represents one possible result that might be obtained if the entire study were repeated, including selecting a new panel (which very likely might contain some members of the existing panel). By repeating the simulation multiple times, a bootstrap distribution for the statistical measures of the hazard can be obtained.

The bootstrap approach was applied to the development of the aggregate hazard distribution. One thousand simulations of aggregate distributions were computed by randomly sampling, with replacement, 10 experts from the panel. For each simulation, the mean and the 5th and 95th percentiles of the aggregate hazard distribution were computed. The resulting 1,000 estimates of the hazard statistics were then ordered to form confidence intervals for the three hazard statistics.

These are plotted on Figure 4-38 as horizontal error bars representing the 90-percent bounds of the simulated distributions (5^{th} to 95^{th} percentiles) for the hazard statistics. The dots are plotted at the medians. The resulting 90-percent intervals show similar characteristics to those obtained from the subset analysis and indicate stability of the results.

The conclusion that can be drawn is that we would not expect to obtain a significantly different result upon repeating the entire process. This results from the fact that most of the uncertainty in the estimated hazard arises from the uncertainty that an individual expert has in interpreting the available data rather than from differences between the interpretations of the experts.

4.3 SUMMARY

The results of the PVHA analysis are that the aggregate expected annual frequency of intersection of the repository footprint by a volcanic event is $1.5 \cdot 10^{-8}$, with a 90-percent confidence interval of $5.4 \cdot 10^{-10}$ to $4.9 \cdot 10^{-8}$. The major contributions to the uncertainty in the frequency of intersection are the statistical uncertainty in estimating the rate of volcanic events from small data sets and the uncertainty in modeling the spatial distribution of future events. Although there are significant differences between the interpretations of the 10 experts, most of the uncertainty in the computed frequency of intersection is due to the average uncertainty that an individual expert expressed in developing the appropriate PVHA model.

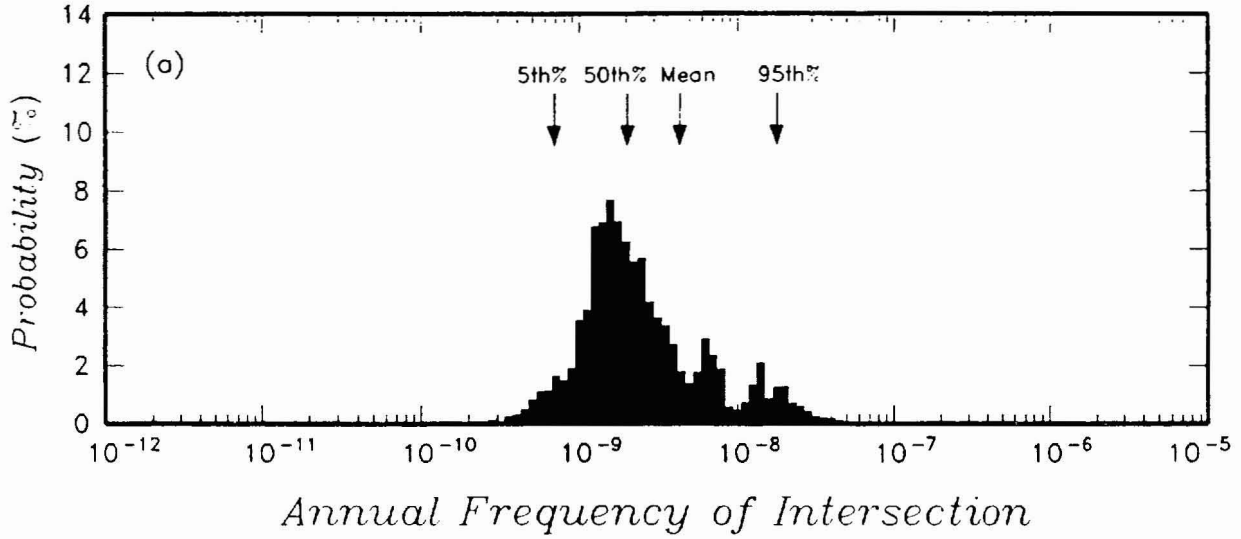

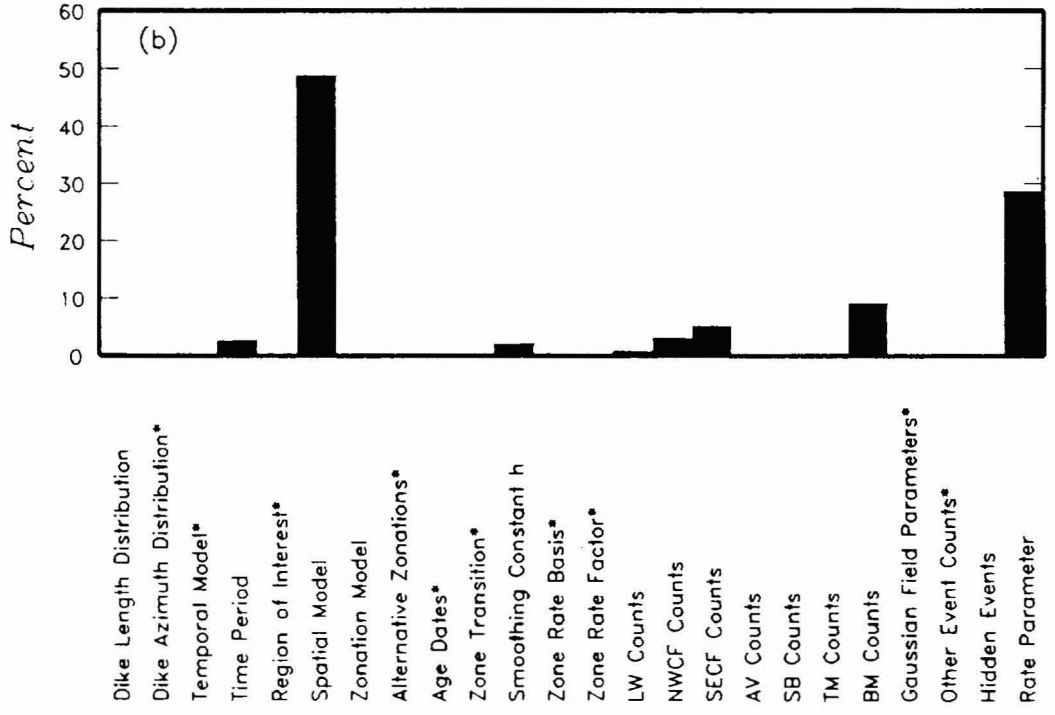

Figure 4-1 PVHA results obtained using Alexander McBirney's PVHA model. (a) Distribution for annual frequency of exceedance. (b) Relative contribution of uncertainty in various components of the PVHA model to the total variance in annual frequency of intersection. Components marked with a * were not treated as uncertain.

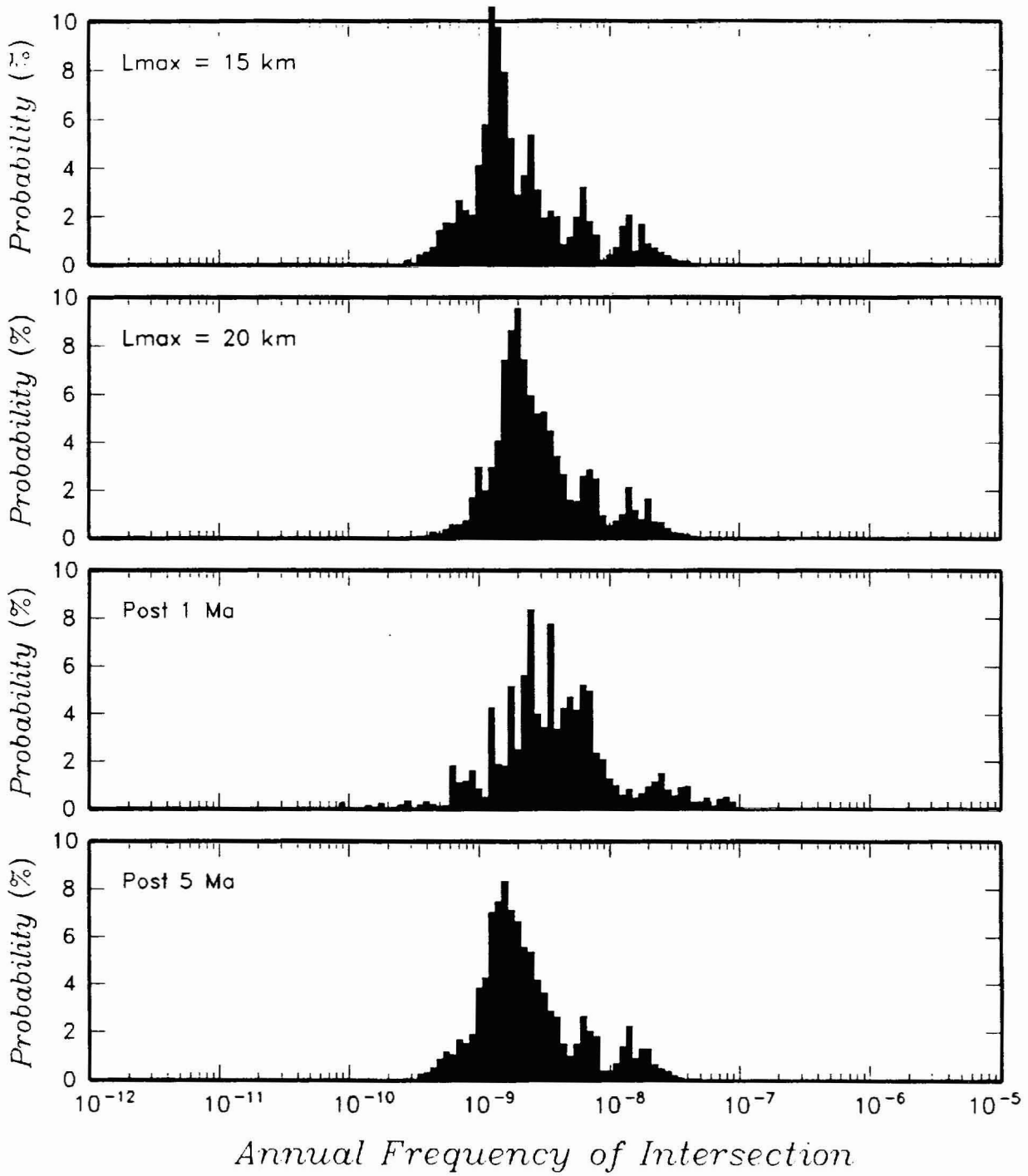

Figure 4-2 Effect of choice of maximum dike length and time period of interest on computed hazard distribution for Alexander McBirney's PVHA model.

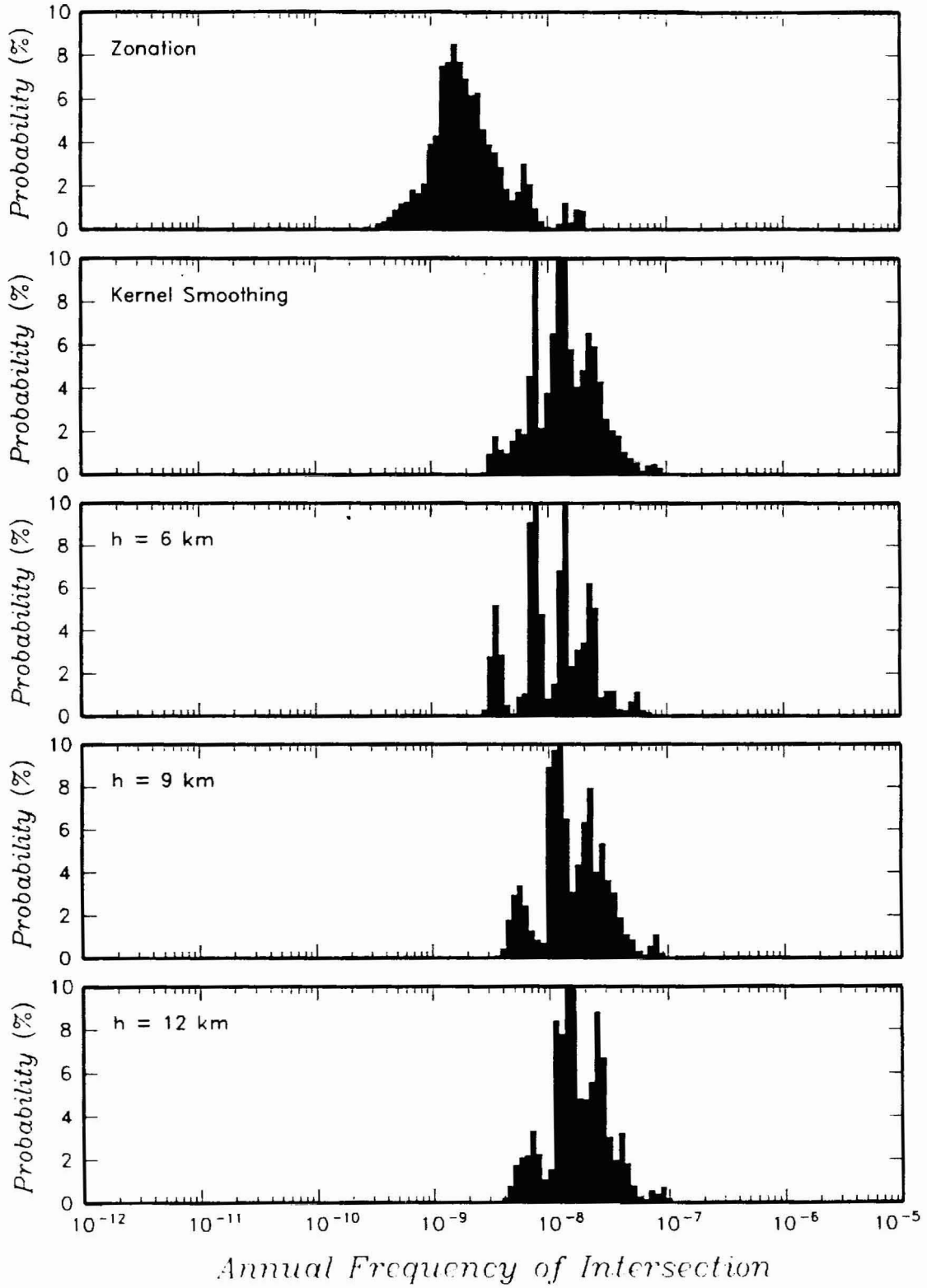

Figure 4-3 Effect of choice of spatial model and smoothing parameter, *h*, on computed hazard distribution for Alexander McBirney's PVHA model.

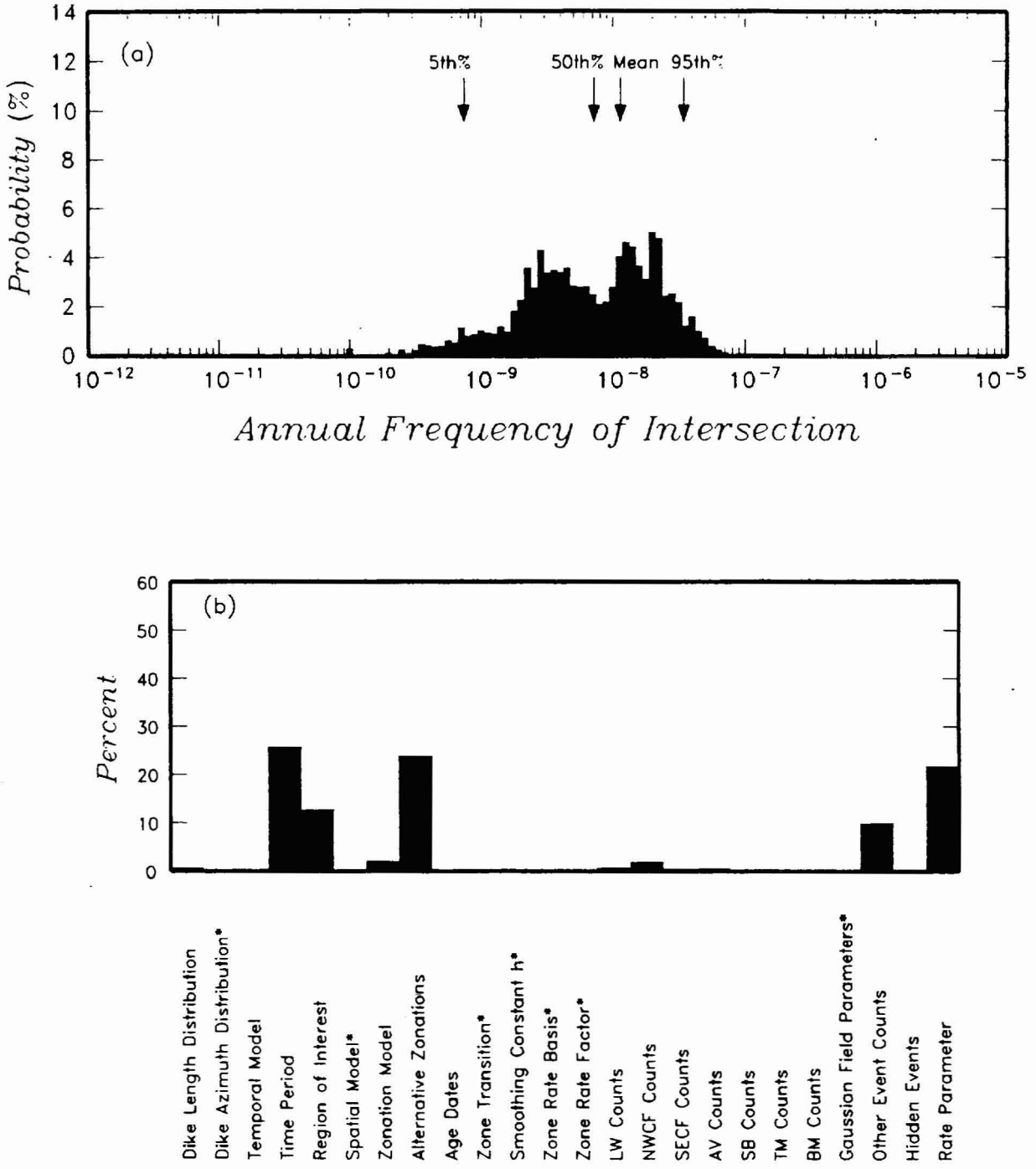

Figure 4-4 PVHA results obtained using Alexander McBirney's PVHA model. (a) Distribution for annual frequency of exceedance. (b) Relative contribution of uncertainty in various components of the PVHA model to the total variance in annual frequency of intersection. Components marked with a * were not treated as uncertain.

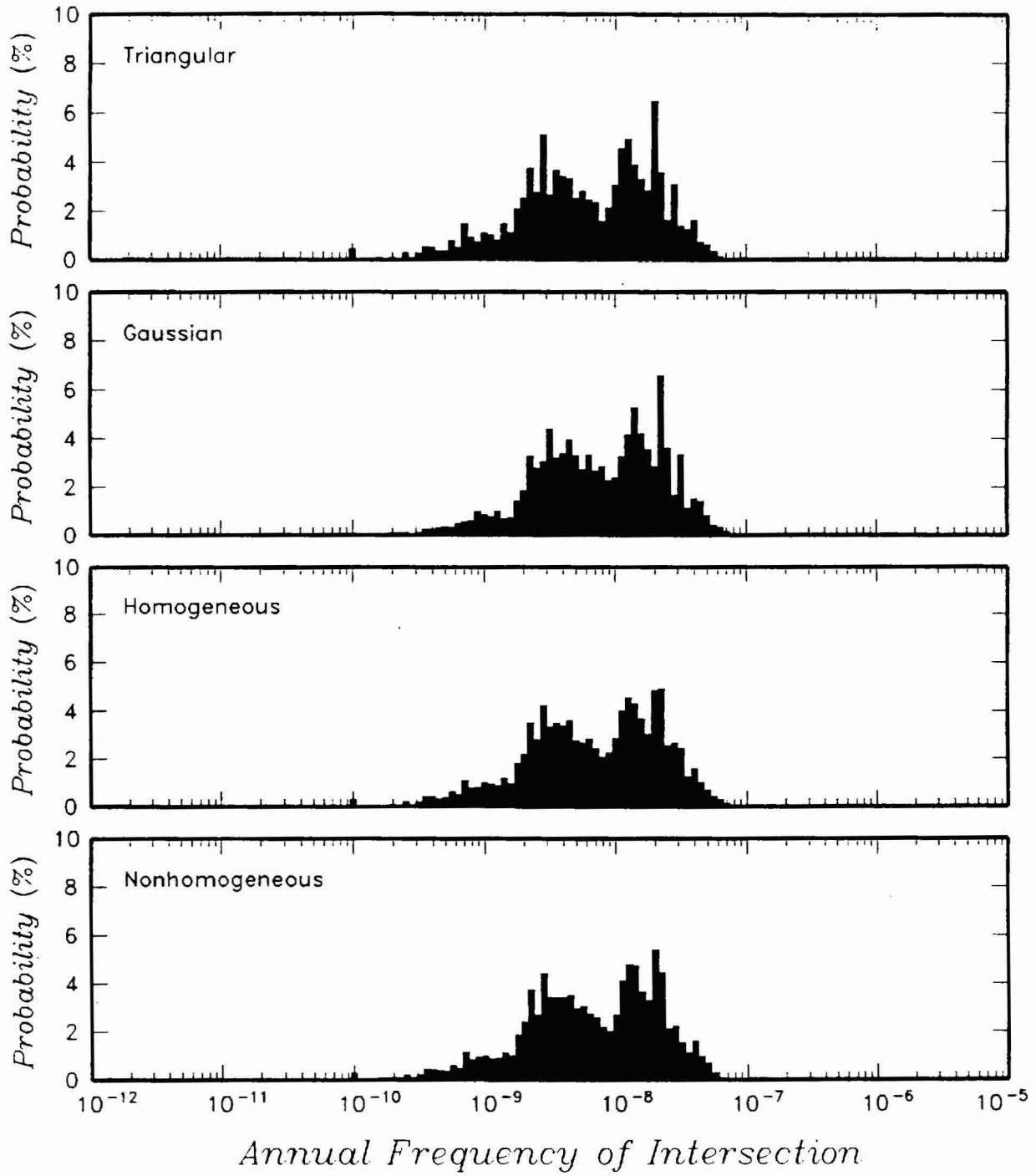

Figure 4-5 Effect of choice of dike length distribution and temporal model on computed hazard distribution for Bruce Crowe's PVHA model.

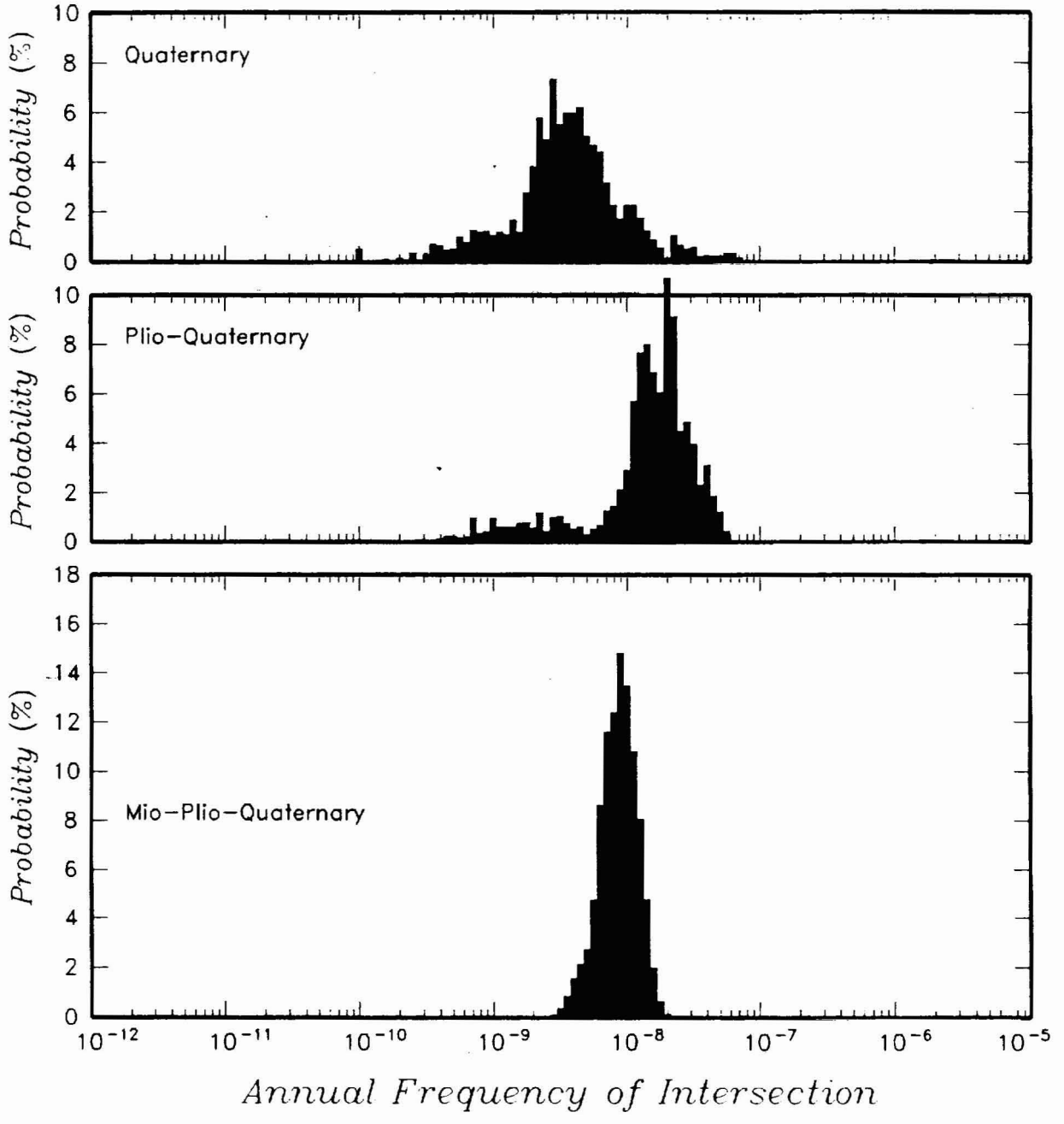

Figure 4-6 Effect of choice of time period on computed hazard distribution for Bruce Crowe's PVHA model.

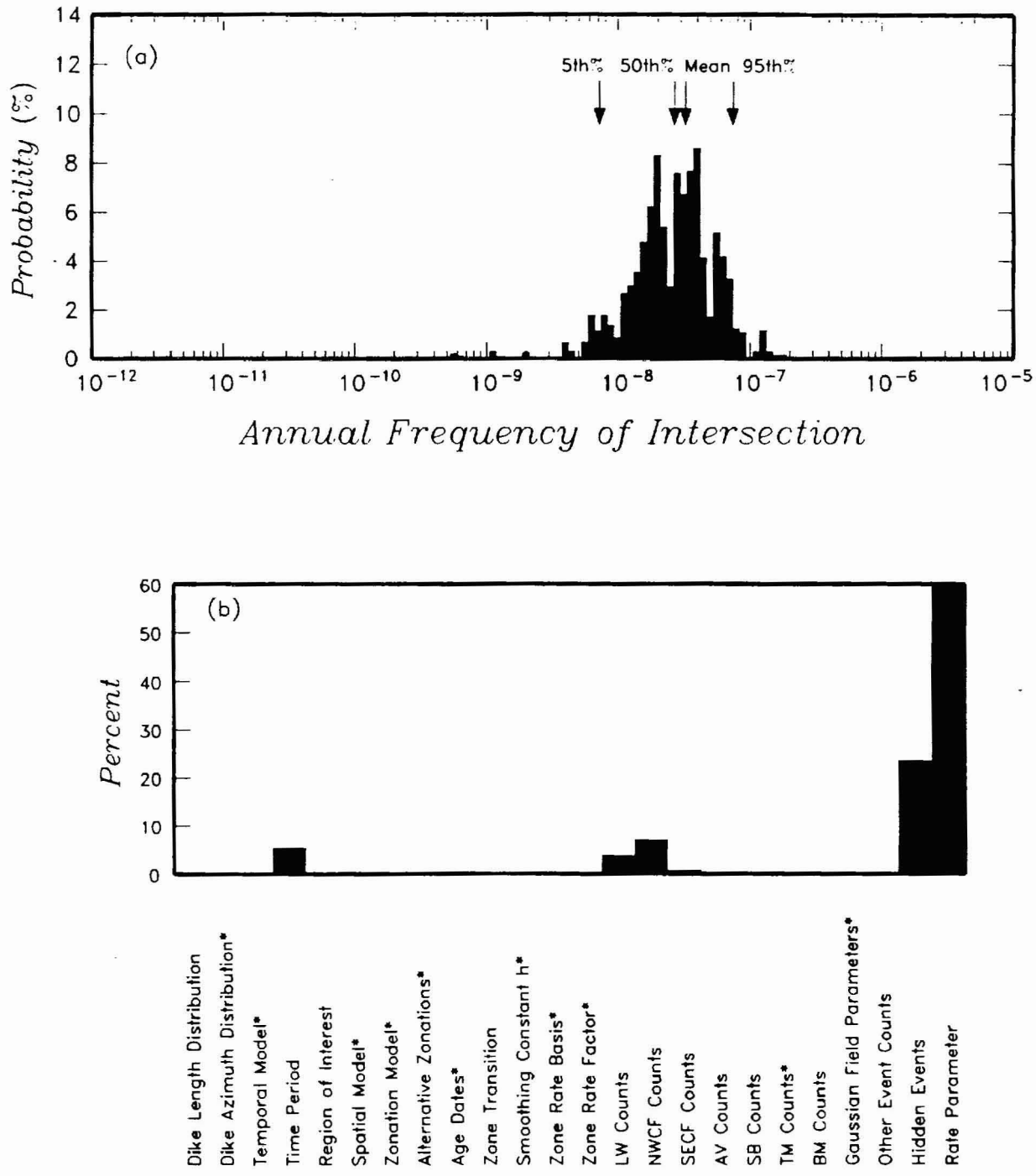

Figure 4-7 PVHA results obtained using George Thompson's PVHA model. (a) Distribution for annual frequency of exceedance. (b) Relative contribution of uncertainty in various components of the PVHA model to the total variance in annual frequency of intersection. Components marked with a * were not treated as uncertain.

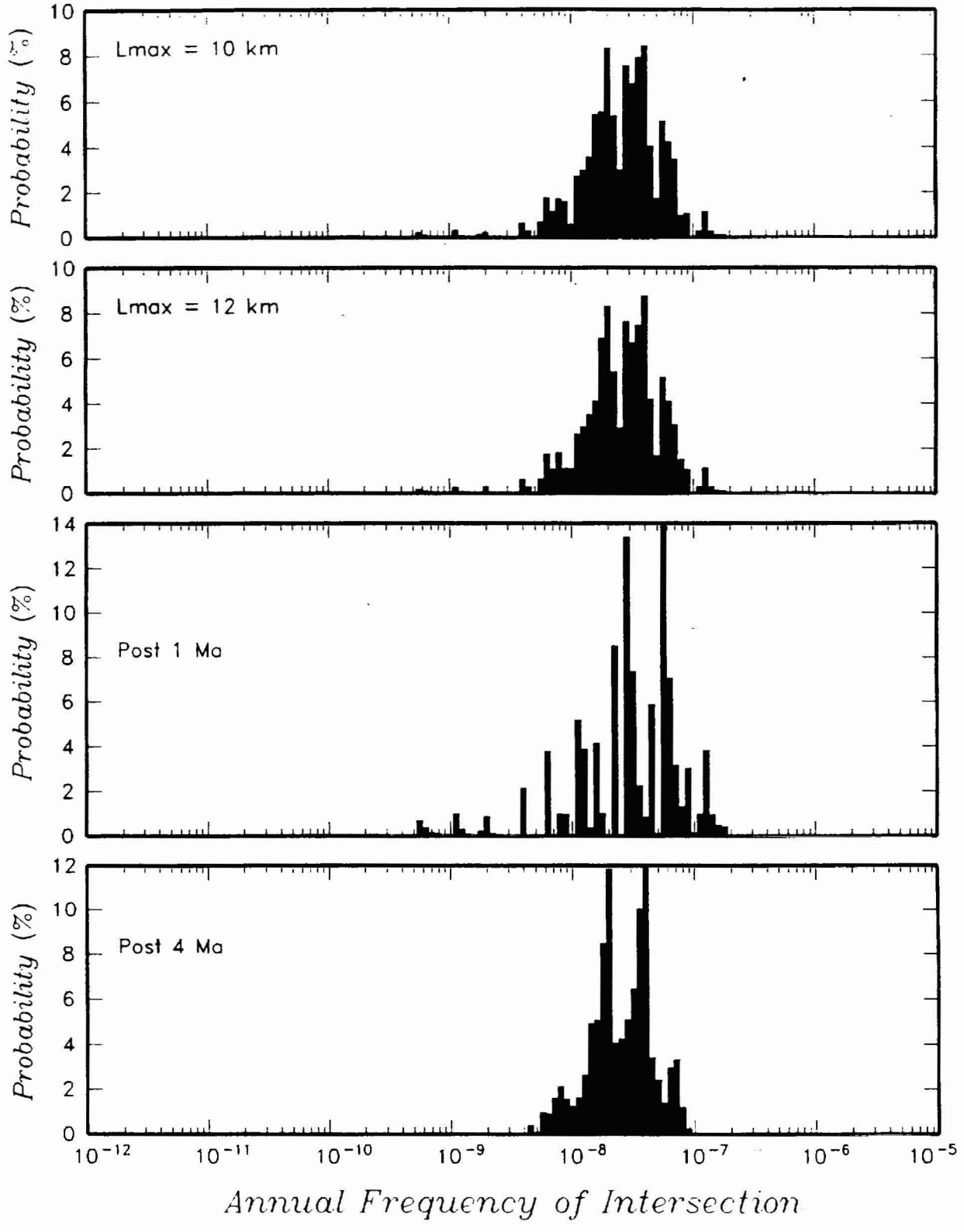

Figure 4-8 Effect of choice of maximum dike length and time period of interest on computed hazard distribution for George Thompson's PVHA model.

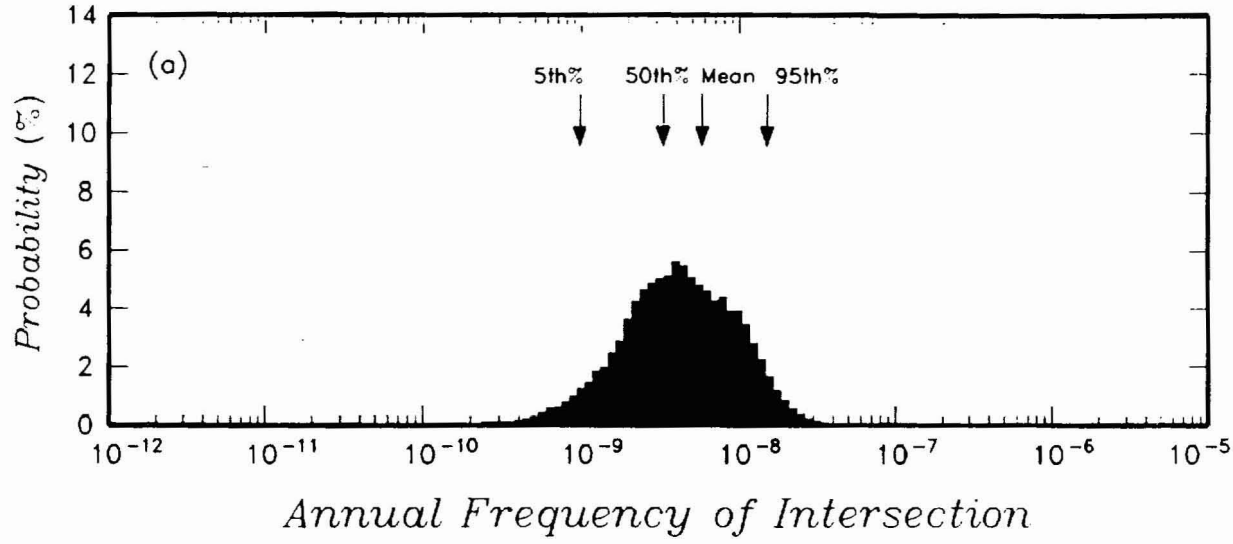

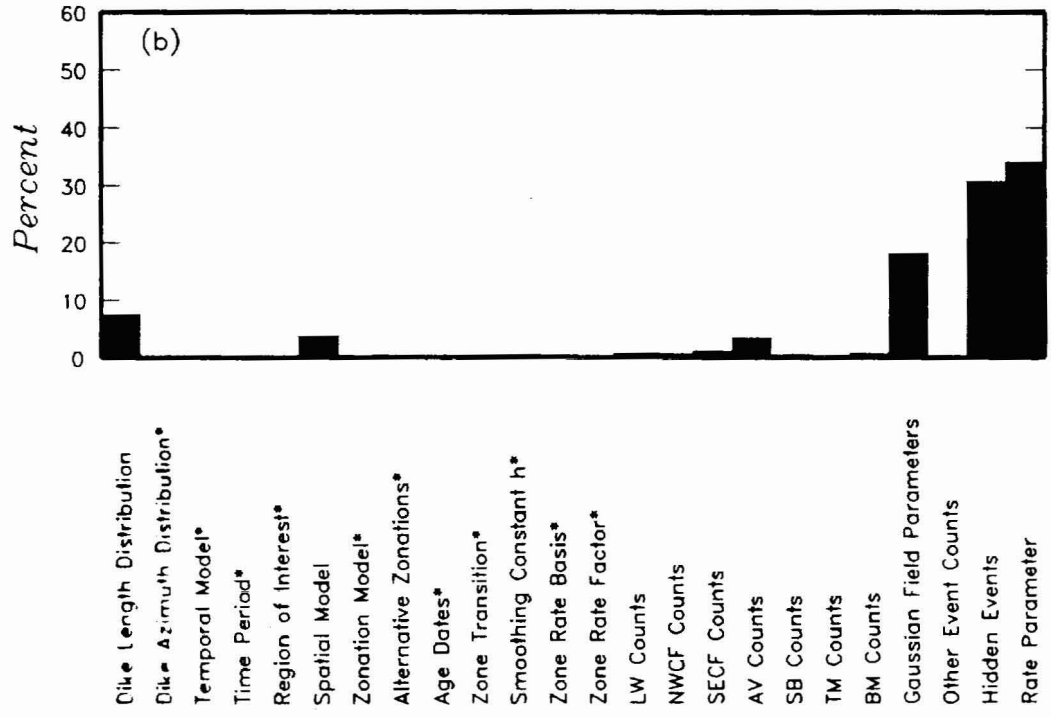

Figure 4-9 PVHA results obtained using George Walker's PVHA model. (a) Distribution for annual frequency of exceedance. (b) Relative contribution of uncertainty in various components of the PVHA model to the total variance in annual frequency of intersection. Components marked with a * were not treated as uncertain.

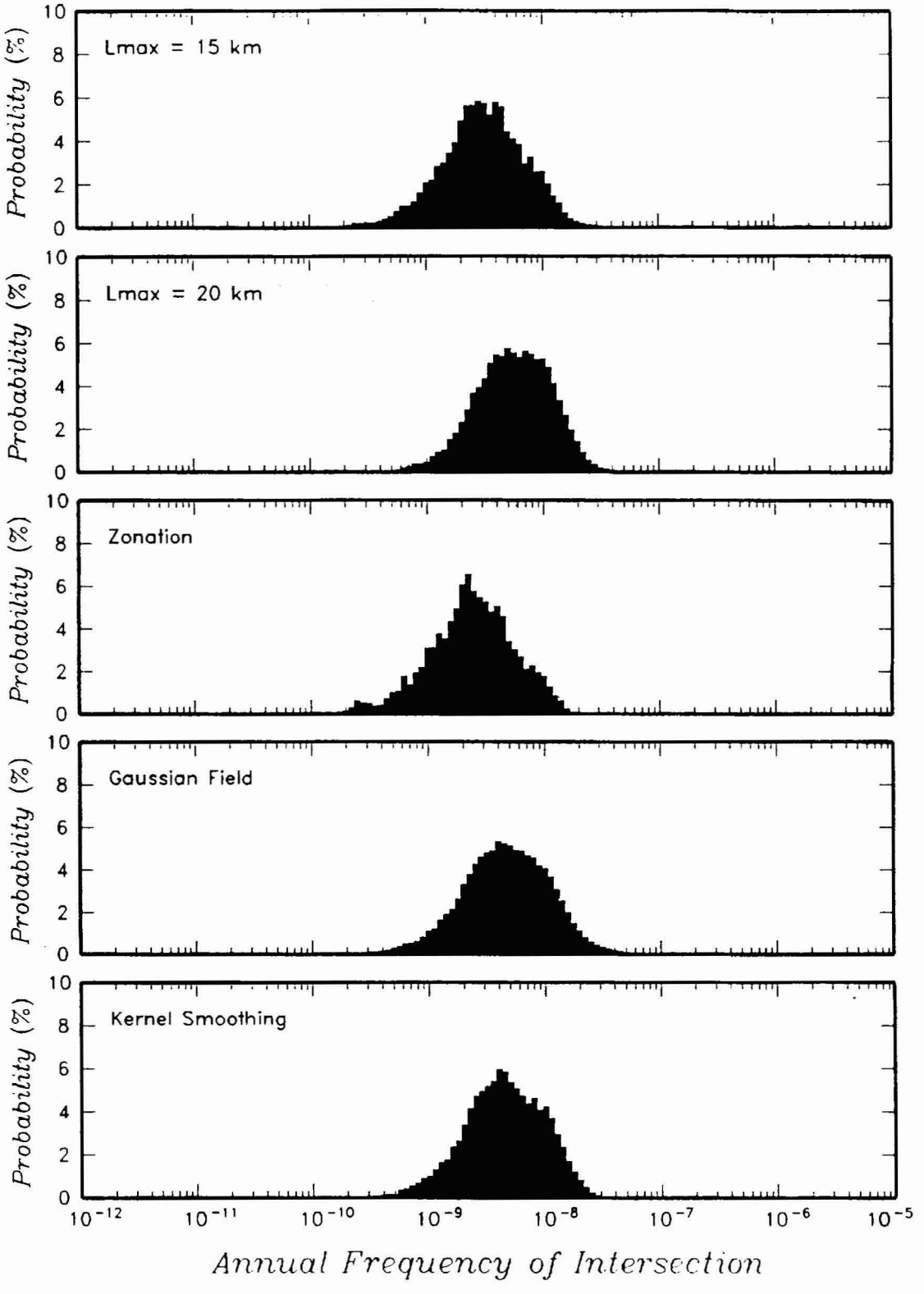

Figure 4-10 Effect of choice of maximum dike length and spatial model on computed hazard distribution for George Walker's PVHA model.

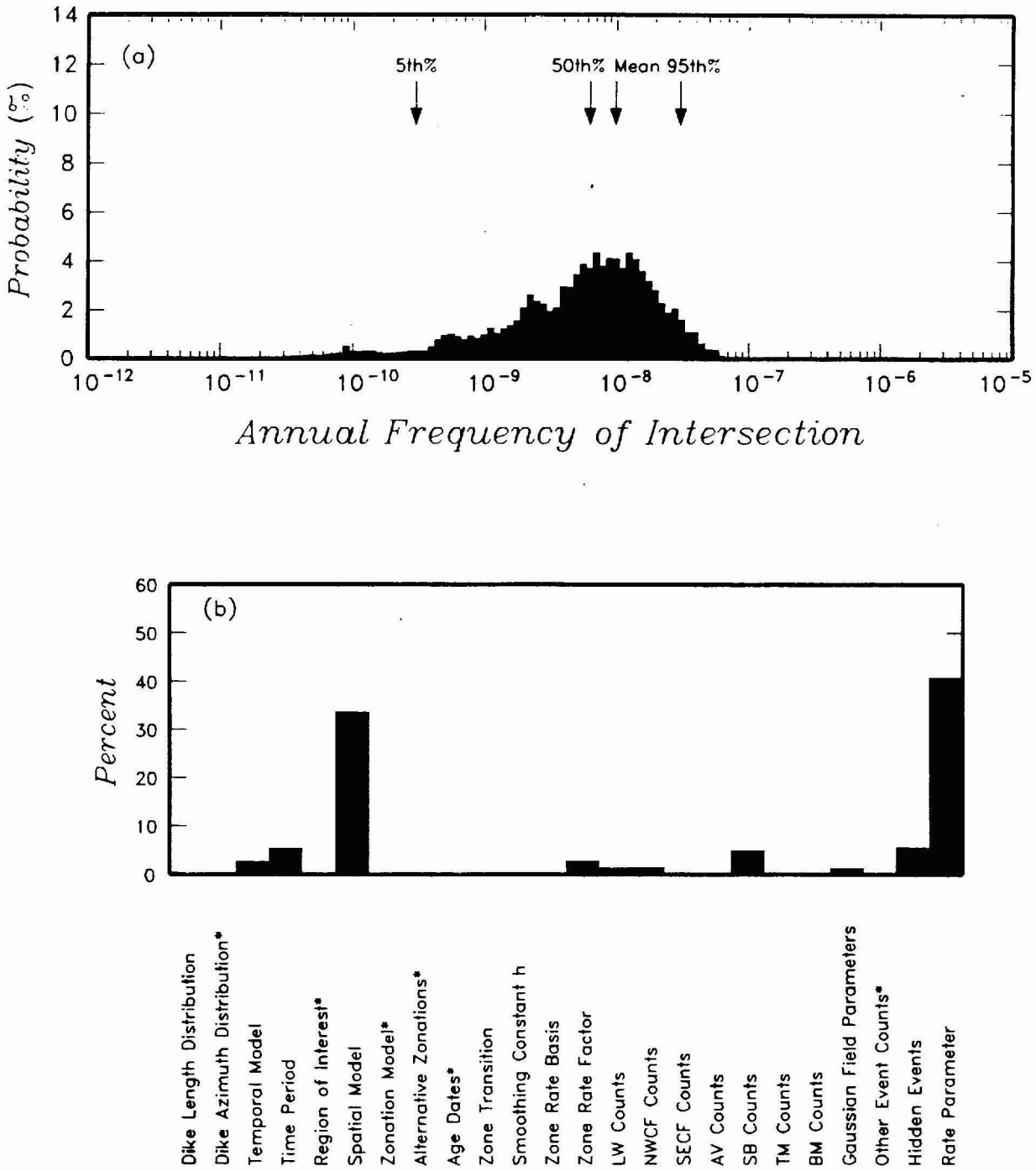

Figure 4-11 PVHA results obtained using Mel Kuntz's PVHA model. (a) Distribution for annual frequency of exceedance. (b) Relative contribution of uncertainty in various components of the PVHA model to the total variance in annual frequency of intersection. Components marked with a * were not treated as uncertain.

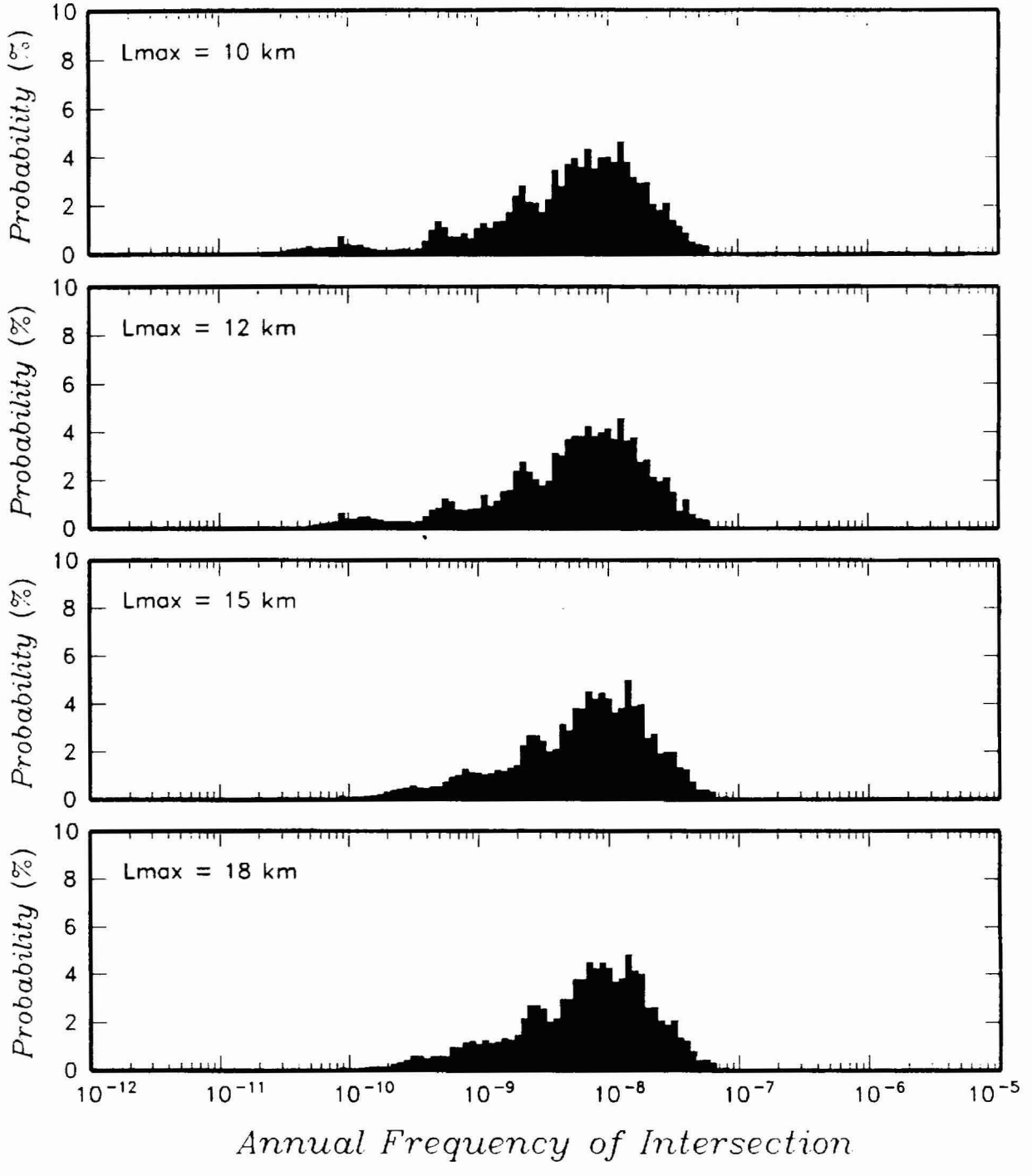

Figure 4-12 Effect of choice of maximum dike length on computed hazard distribution for Mel Kuntz's PVHA model.

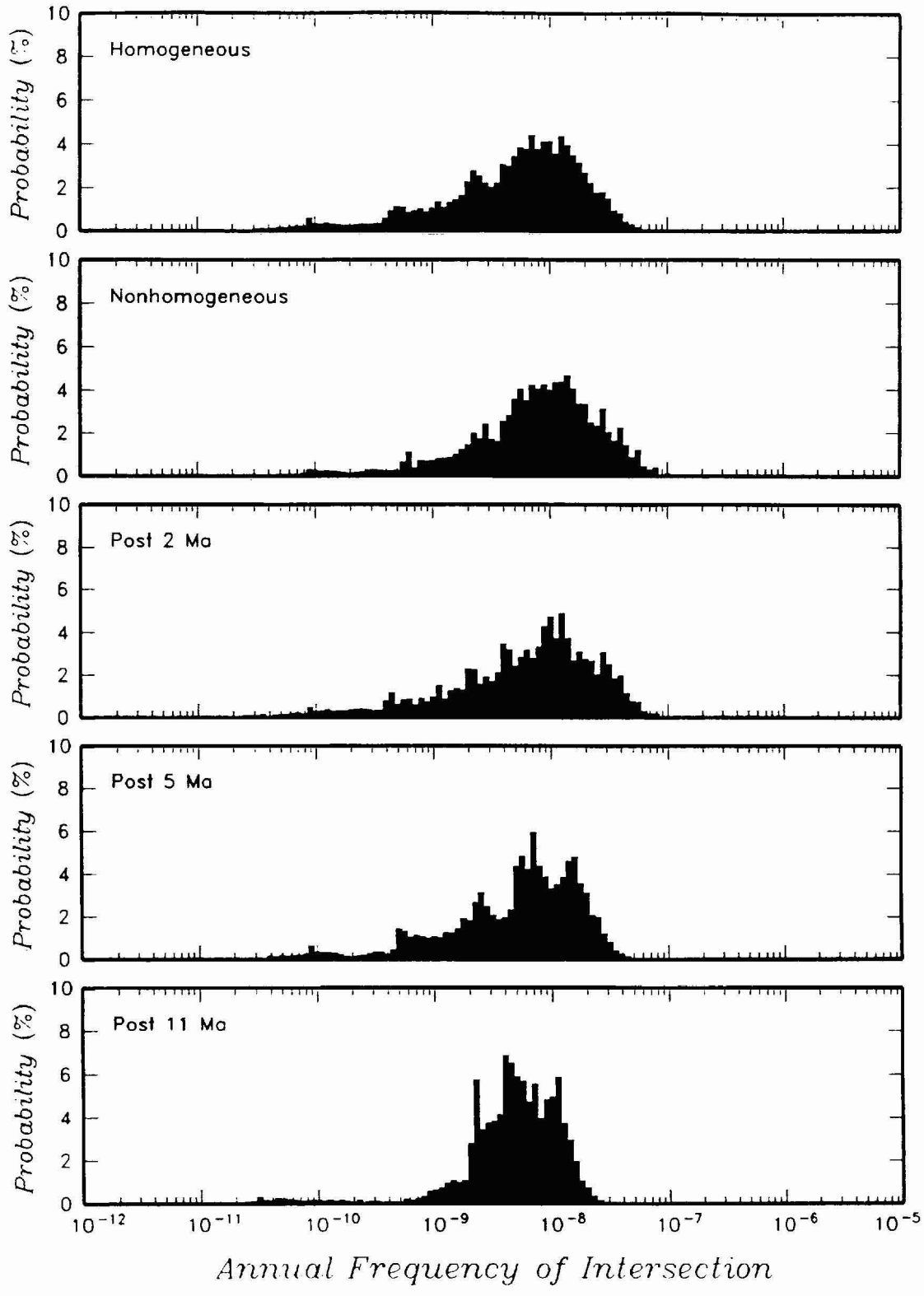

Figure 4-13 Effect of choice of temporal model and time period of interest on computed hazard distribution for Mel Kuntz's PVHA model.

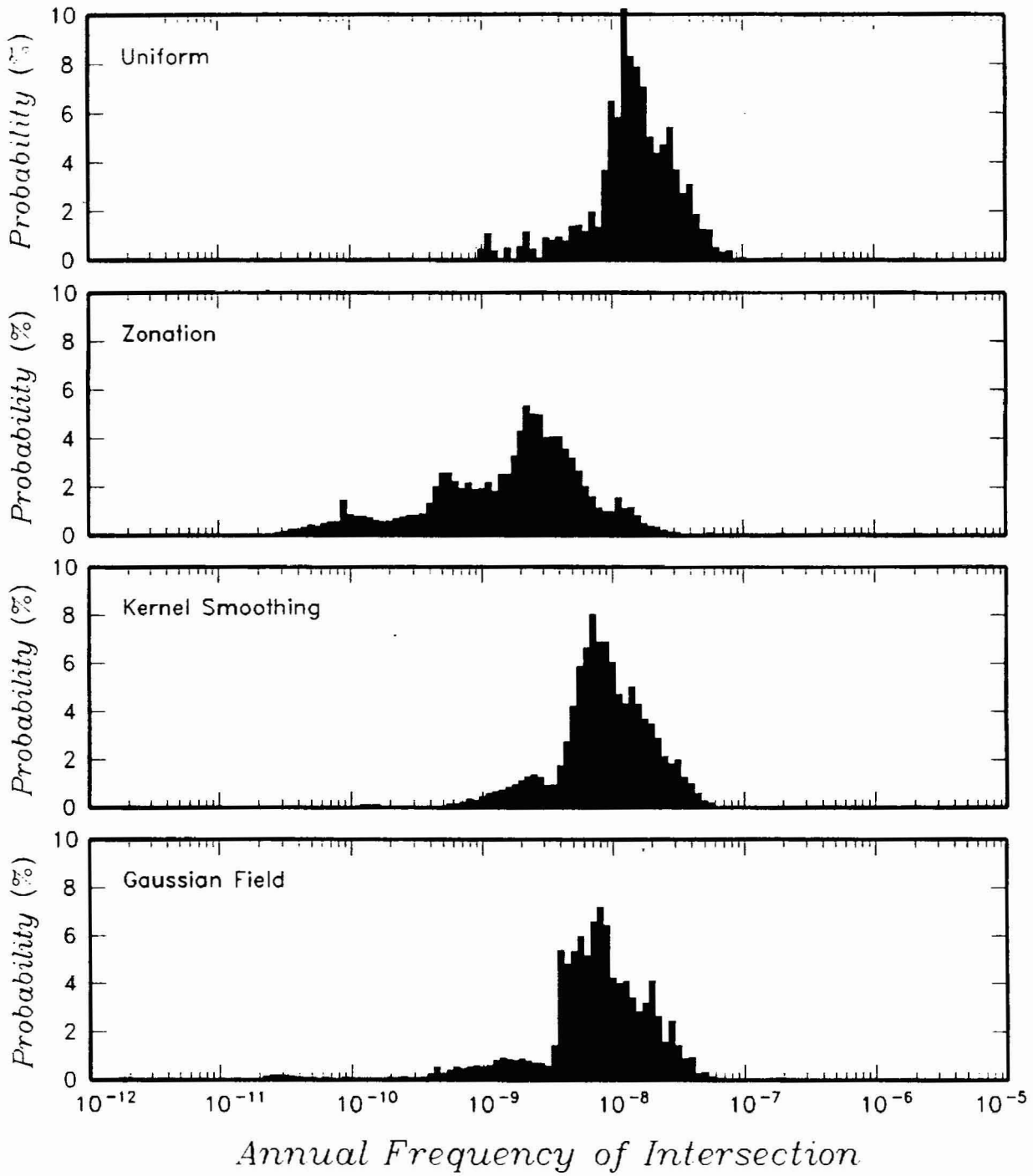

Figure 4-14 Effect of choice of spatial model on computed hazard distribution for Mel Kuntz's PVHA model.

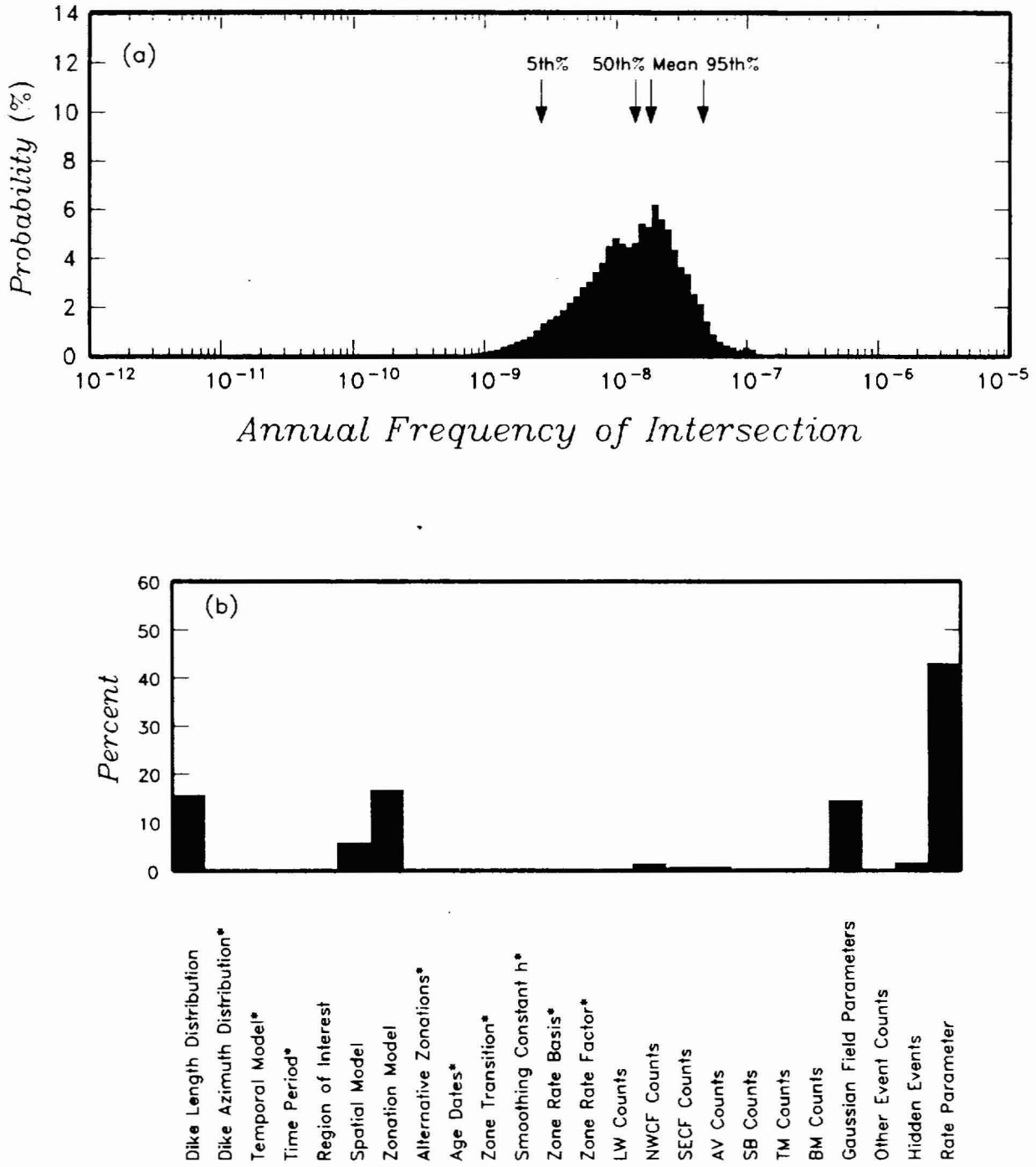

Figure 4-15 PVHA results obtained using Michael Sheridan's PVHA model. (a) Distribution for annual frequency of exceedance. (b) Relative contribution of uncertainty in various components of the PVHA model to the total variance in annual frequency of intersection. Components marked with a * were not treated as uncertain.

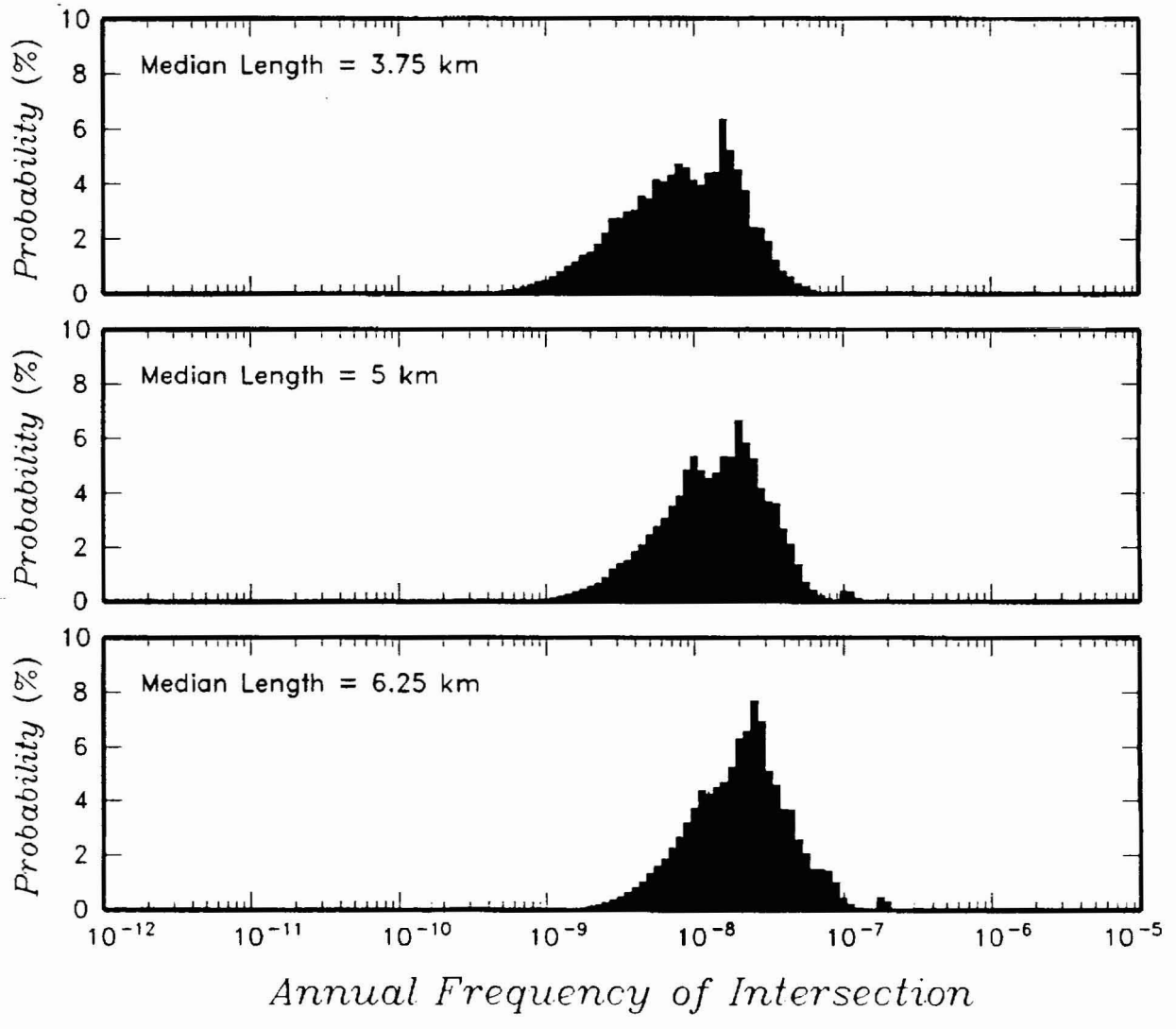

Figure 4-16 Effect of choice of median dike length on computed hazard distribution for Michael Sheridan's PVHA model.

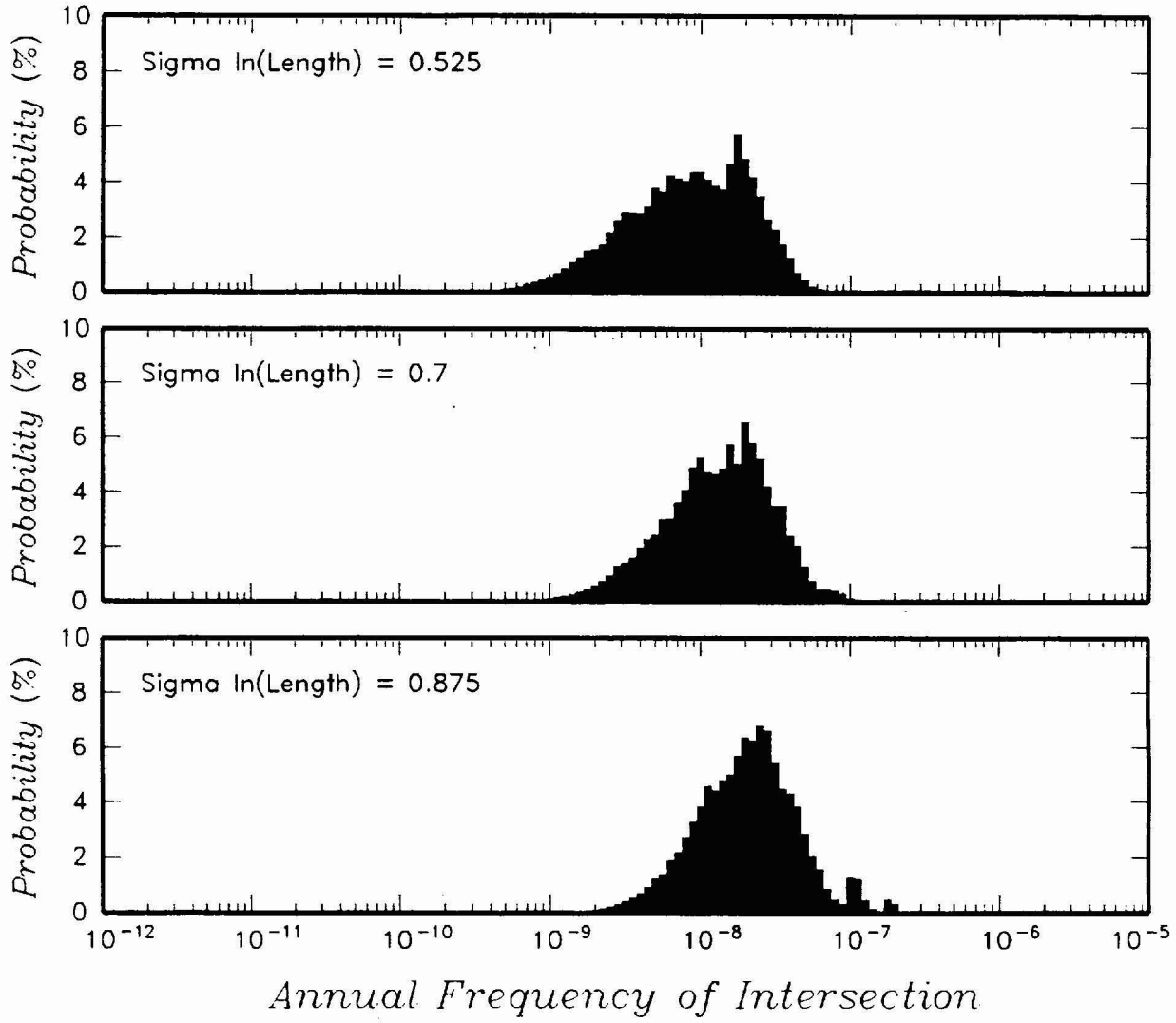

Figure 4-17 Effect of choice of standard error on ln(dike length) on computed hazard distribution for Michael Sheridan's PVHA model.

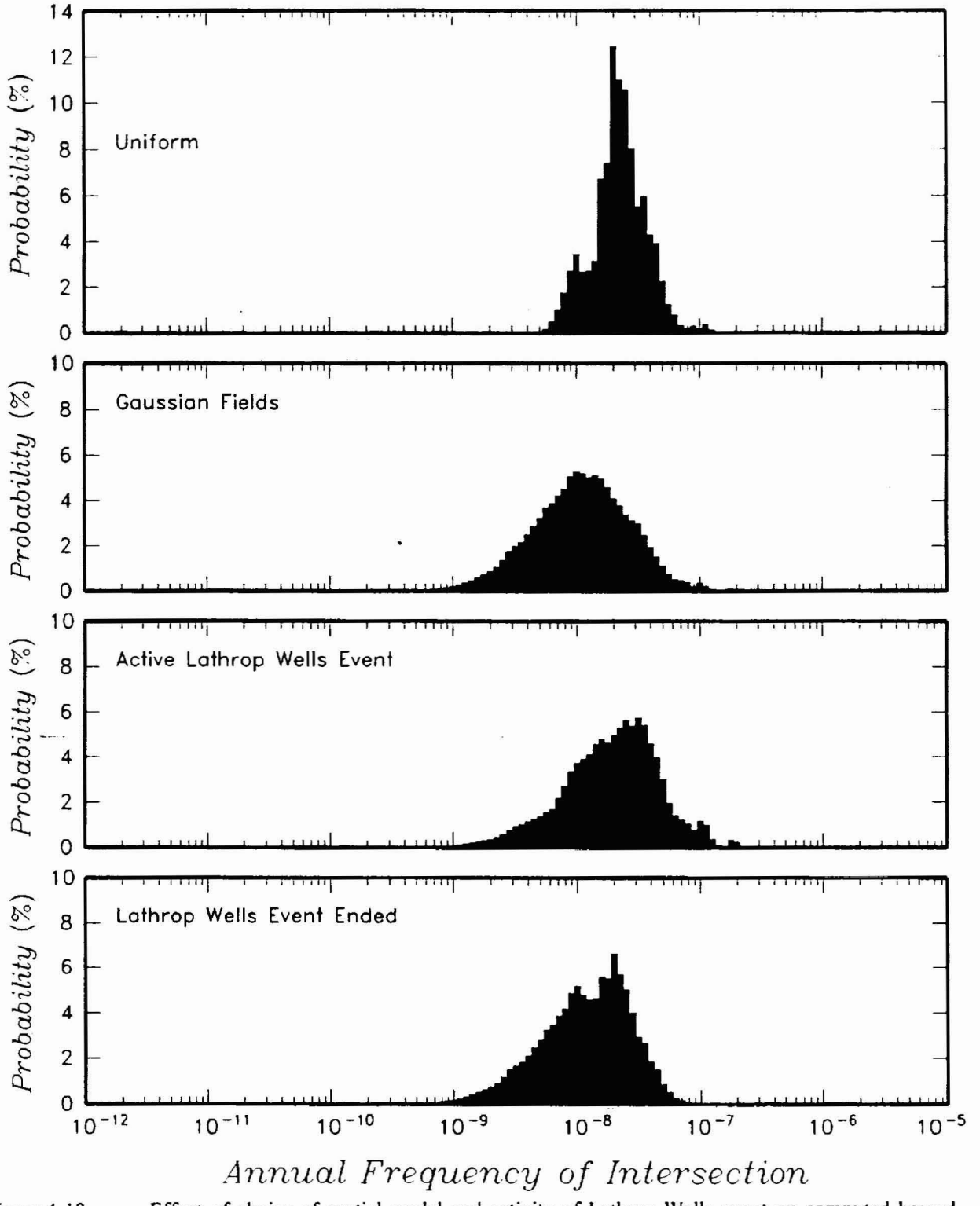

Figure 4-18 Effect of choice of spatial model and activity of Lathrop Wells event on computed hazard distribution for Michael Sheridan's PVHA model.

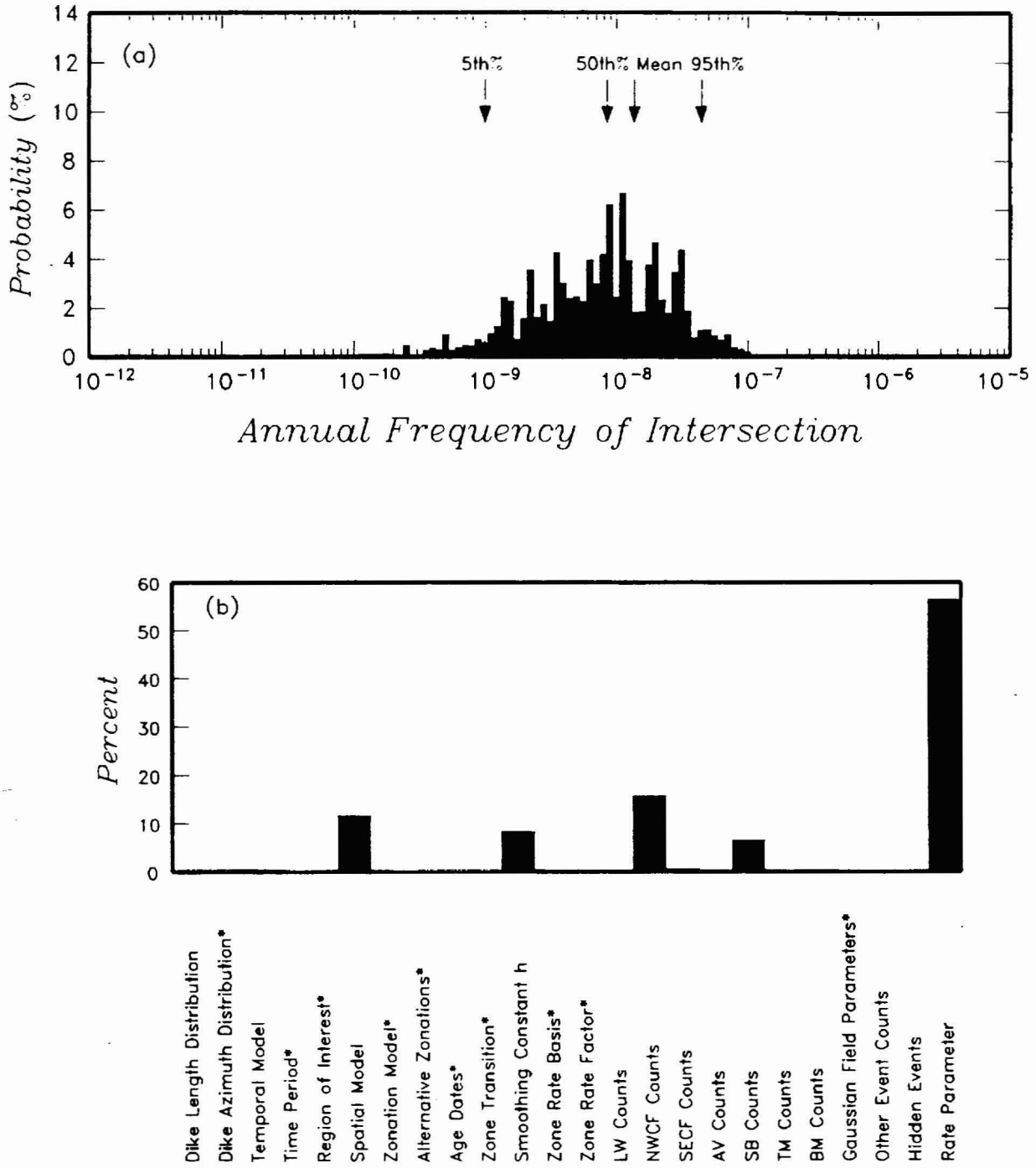

Figure 4-19 PVHA results obtained using Richard Carlson's PVHA model. (a) Distribution for annual frequency of exceedance. (b) Relative contribution of uncertainty in various components of the PVHA model to the total variance in annual frequency of intersection. Components marked with a * were not treated as uncertain.

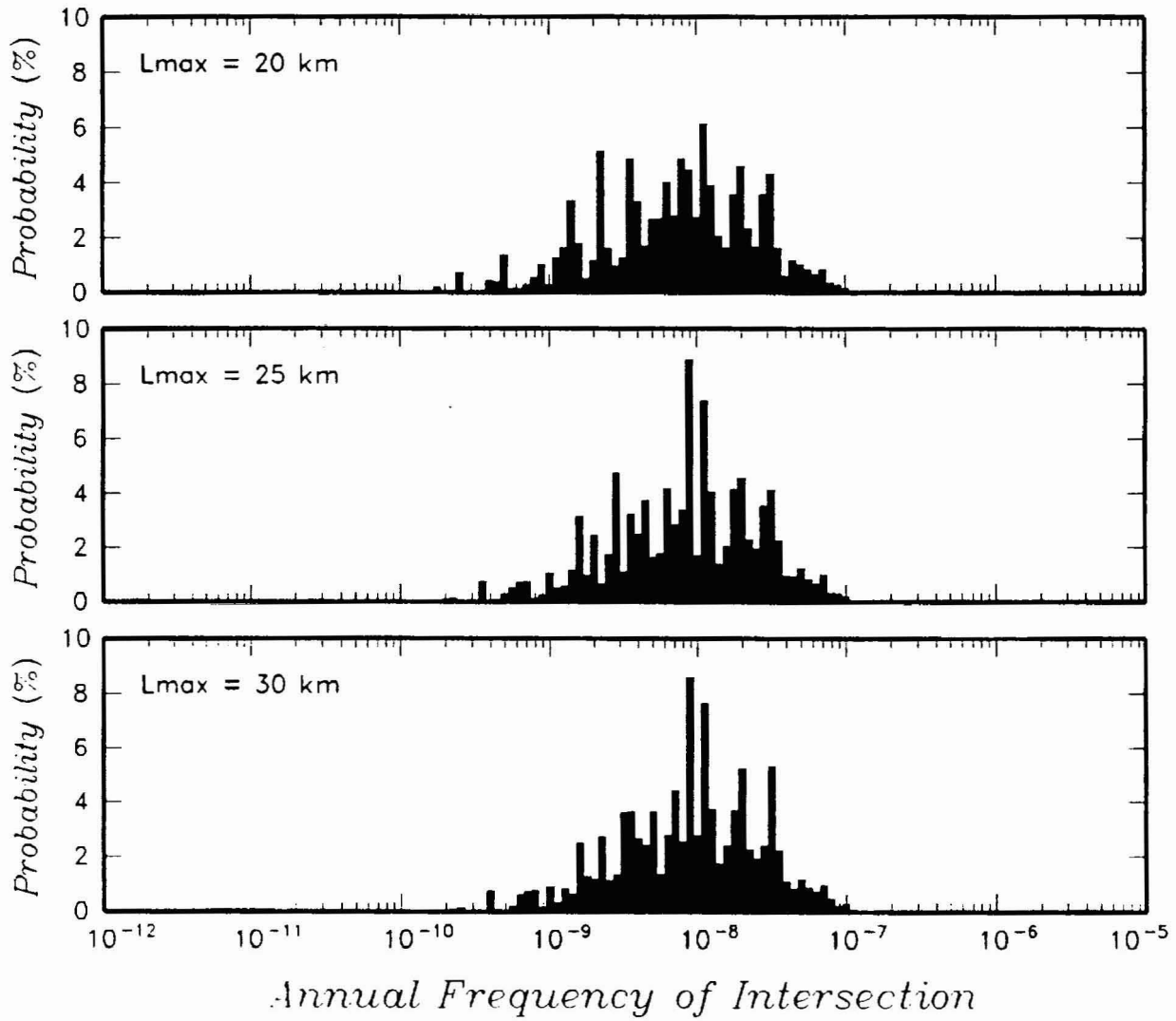

Figure 4-20 Effect of choice of maximum dike length on computed hazard distribution for Richard Carlson's PVHA model.

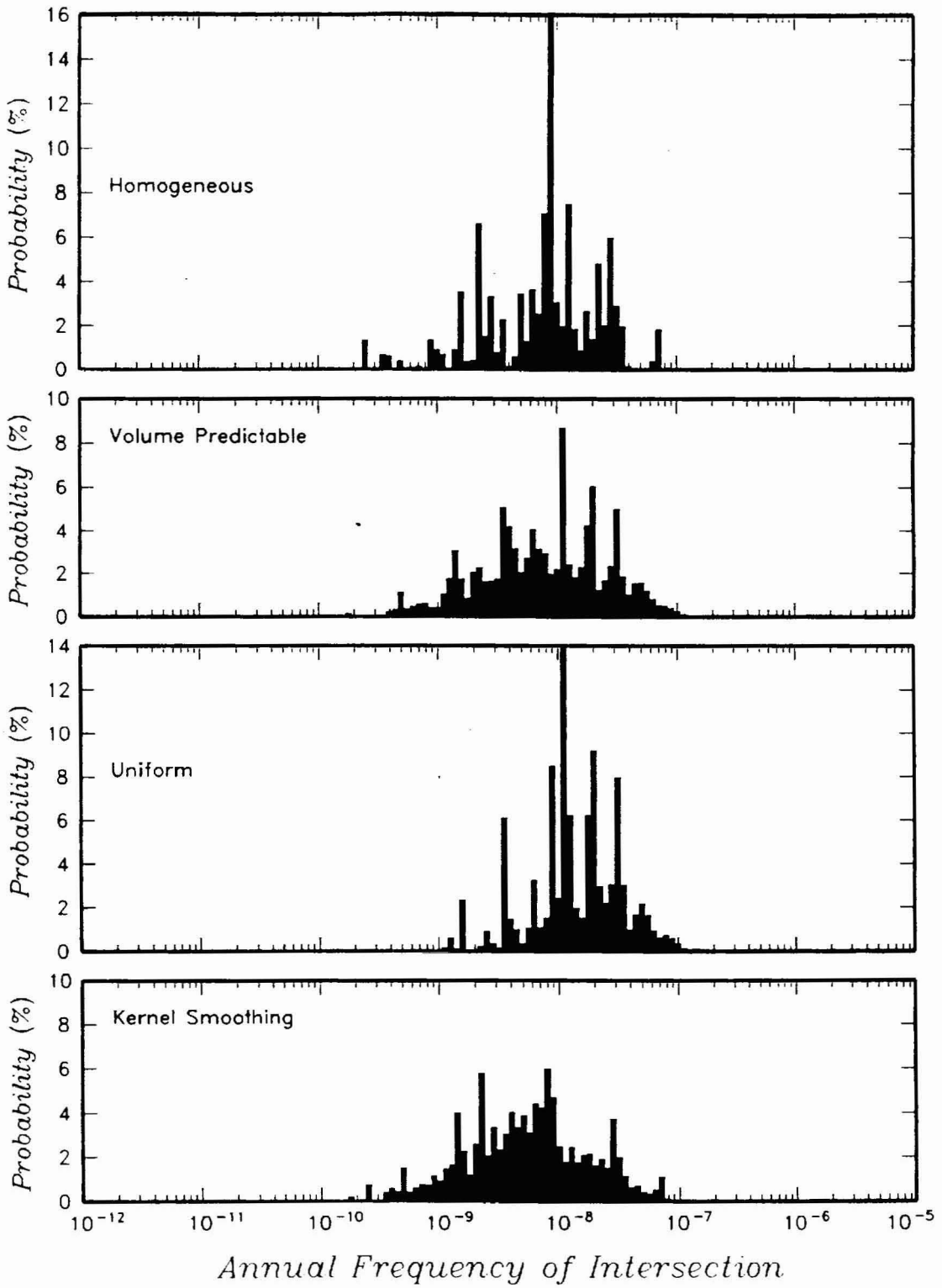

Figure 4-21 Effect of choice of temporal and spatial models on computed hazard distribution for Richard Carlson's PVHA model.

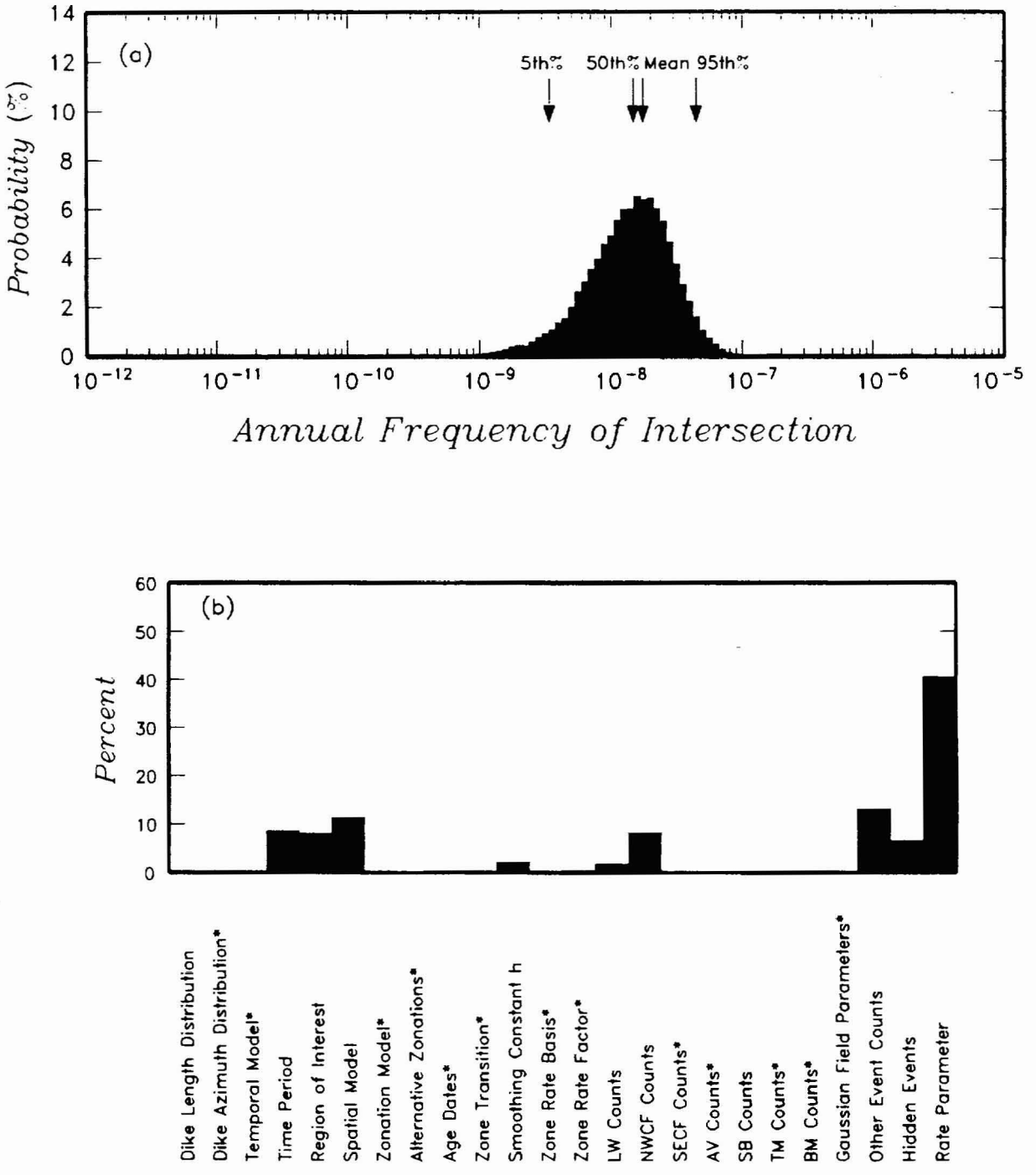

Figure 4-22 PVHA results obtained using Richard Fisher's PVHA model. (a) Distribution for annual frequency of exceedance. (b) Relative contribution of uncertainty in various components of the PVHA model to the total variance in annual frequency of intersection. Components marked with a * were not treated as uncertain.

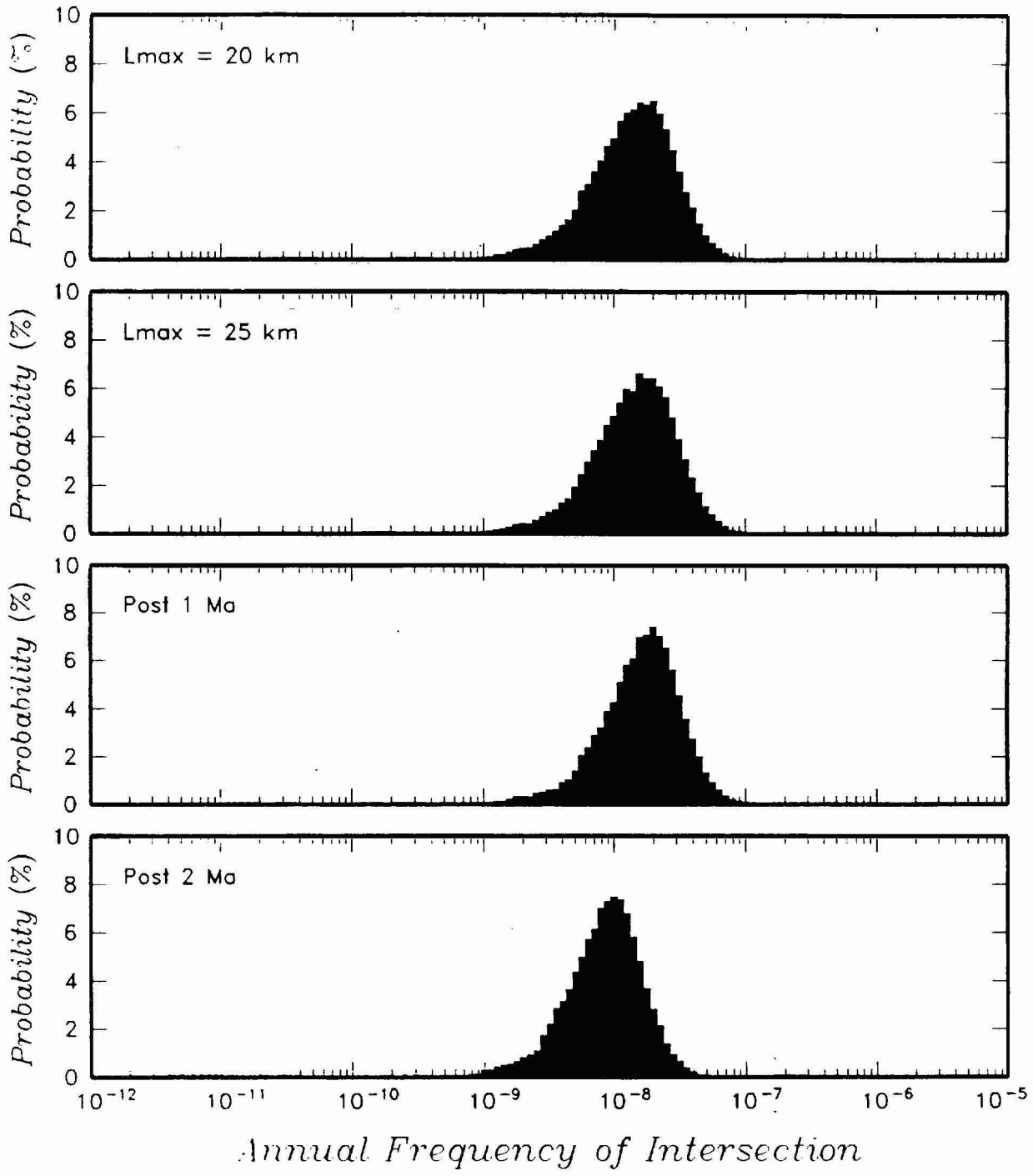

Figure 4-23 Effect of choice of maximum dike length and time period of interest on computed hazard distribution for Richard Fisher's PVHA model.

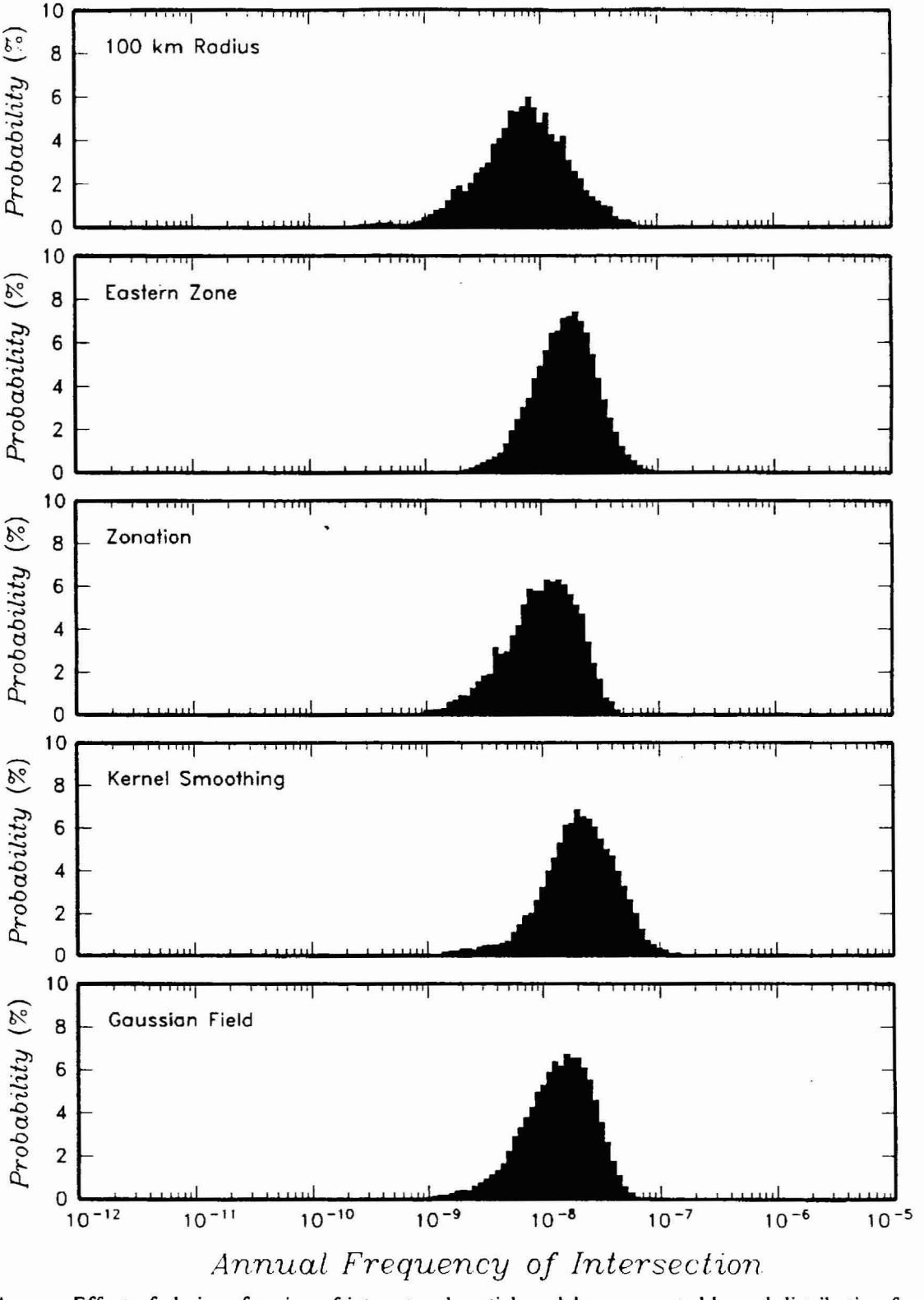

Figure 4-24 Effect of choice of region of interest and spatial model on computed hazard distribution for Richard Fisher's PVHA model.

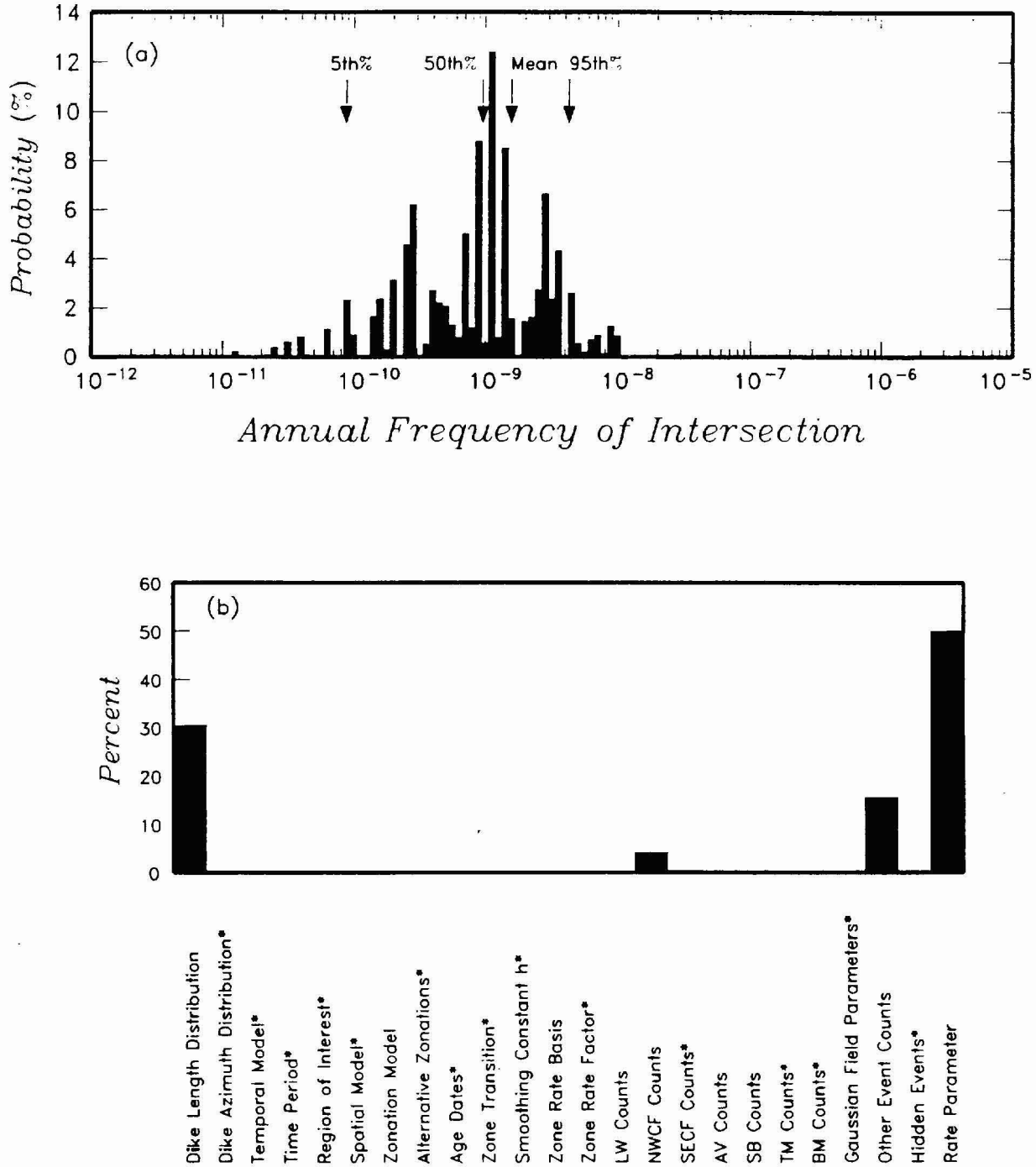

Figure 4-25 PVHA results obtained using Wendell Duffield's PVHA model. (a) Distribution for annual frequency of exceedance. (b) Relative contribution of uncertainty in various components of the PVHA model to the total variance in annual frequency of intersection. Components marked with a * were not treated as uncertain.

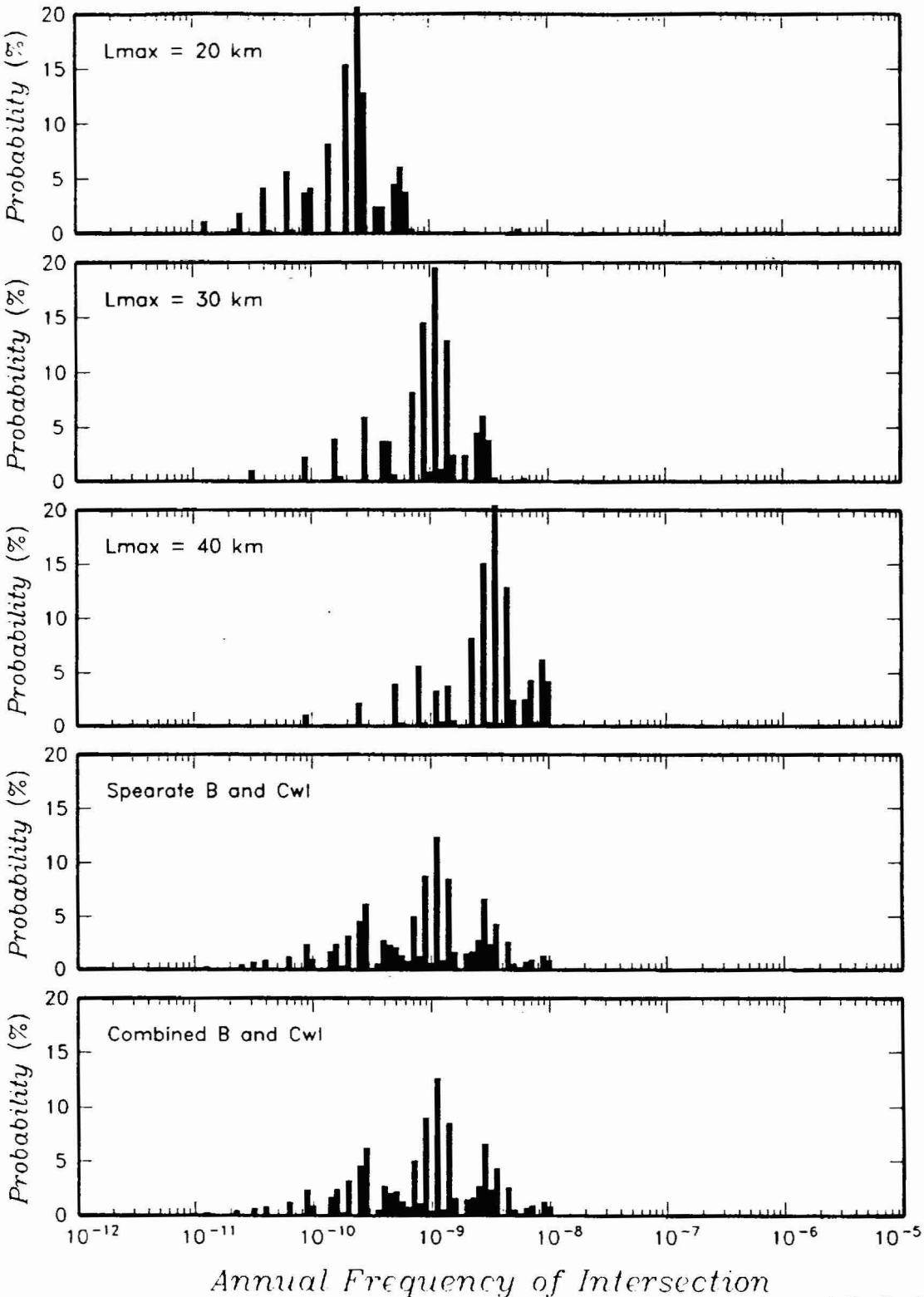

Figure 4-26 Effect of choice of maximum dike length and zonation model on computed hazard distribution for Wendell Duffield's PVHA model.

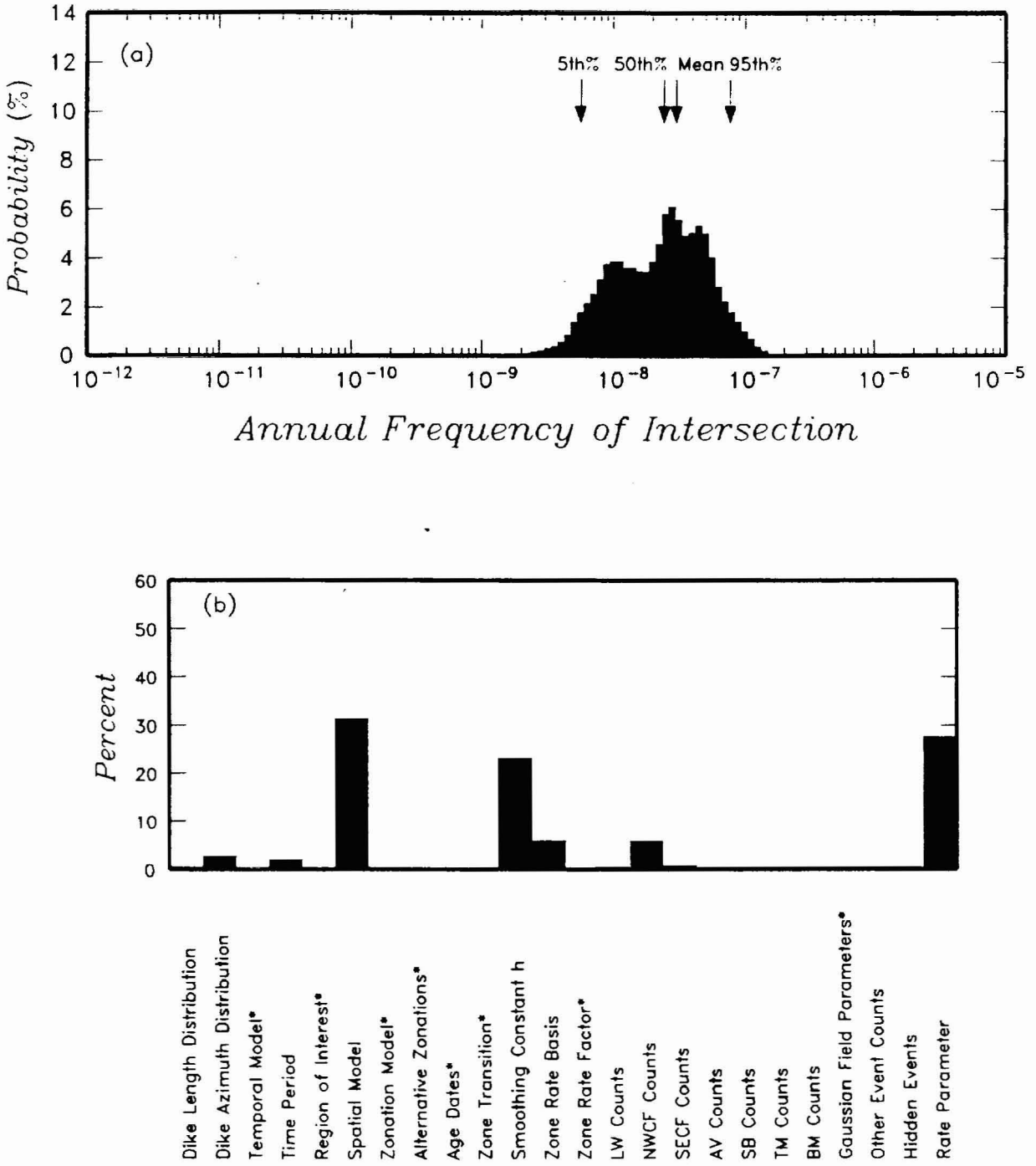

Figure 4-27 PVHA results obtained using William Hackett's PVHA model. (a) Distribution for annual frequency of exceedance. (b) Relative contribution of uncertainty in various components of the PVHA model to the total variance in annual frequency of intersection. Components marked with a * were not treated as uncertain.

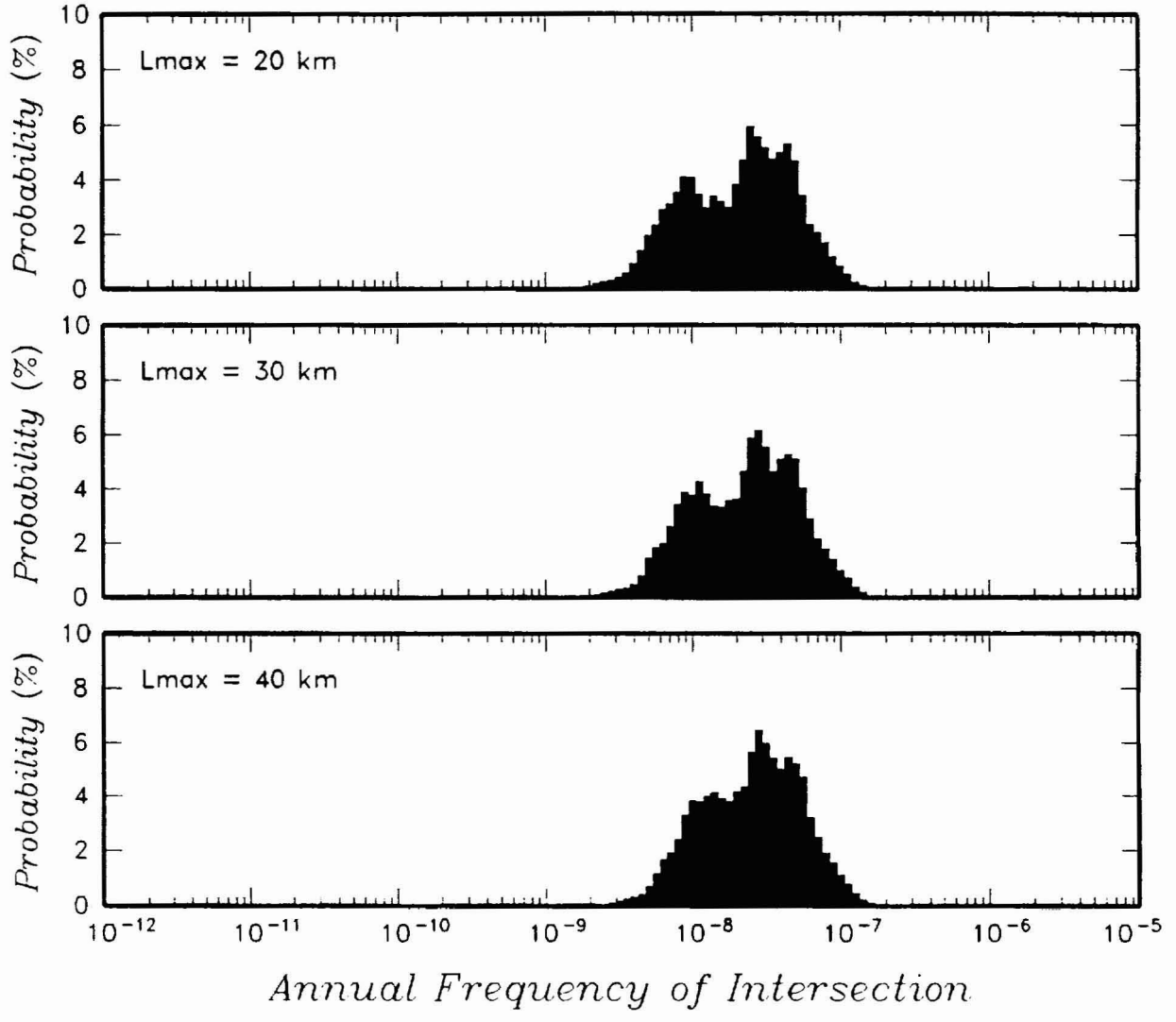

Figure 4-28 Effect of choice of maximum dike length on computed hazard distribution for William Hackett's PVHA model.

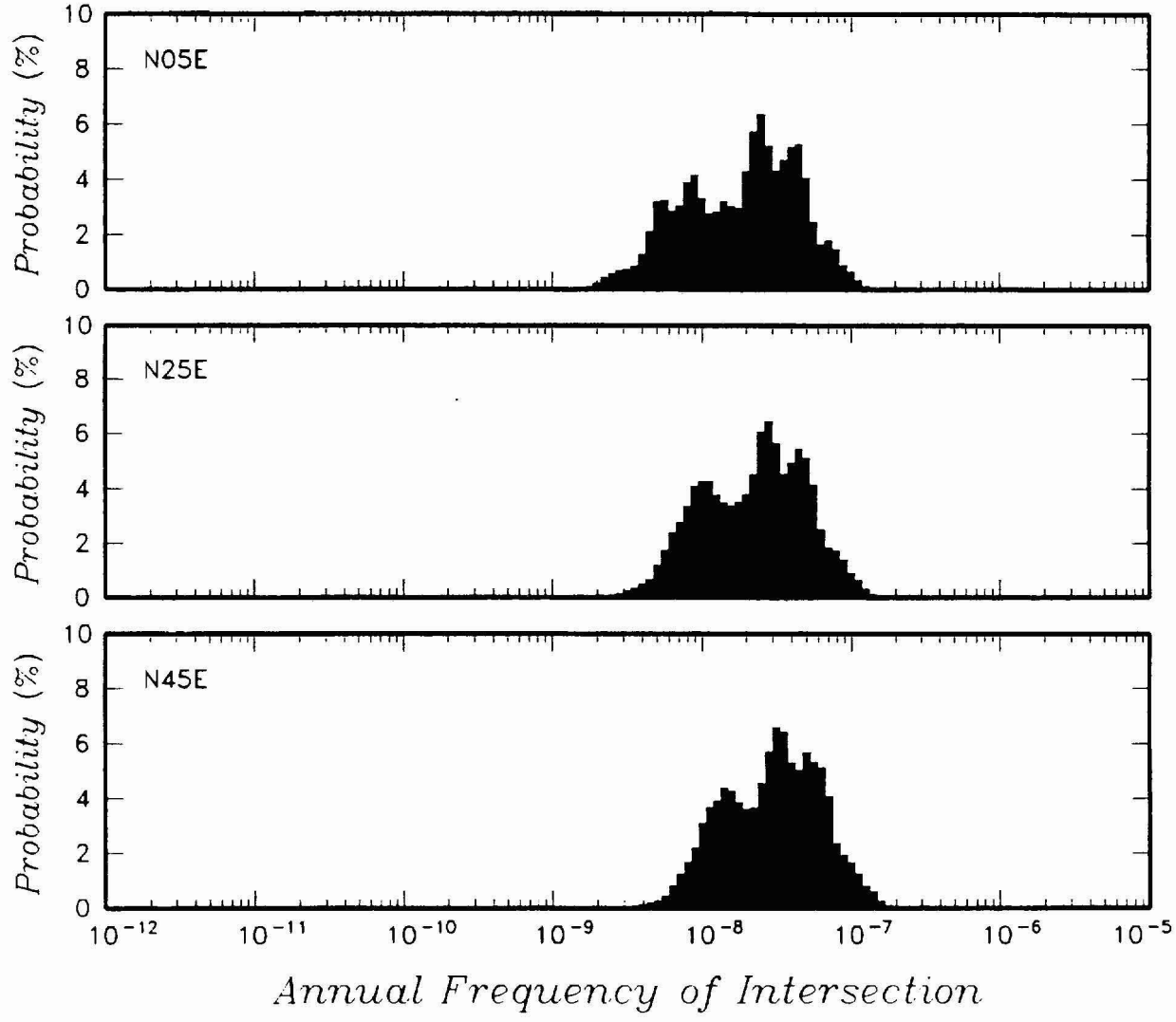

Figure 4-29 Effect of choice of mean dike azimuth on computed hazard distribution for William Hackett's PVHA model.

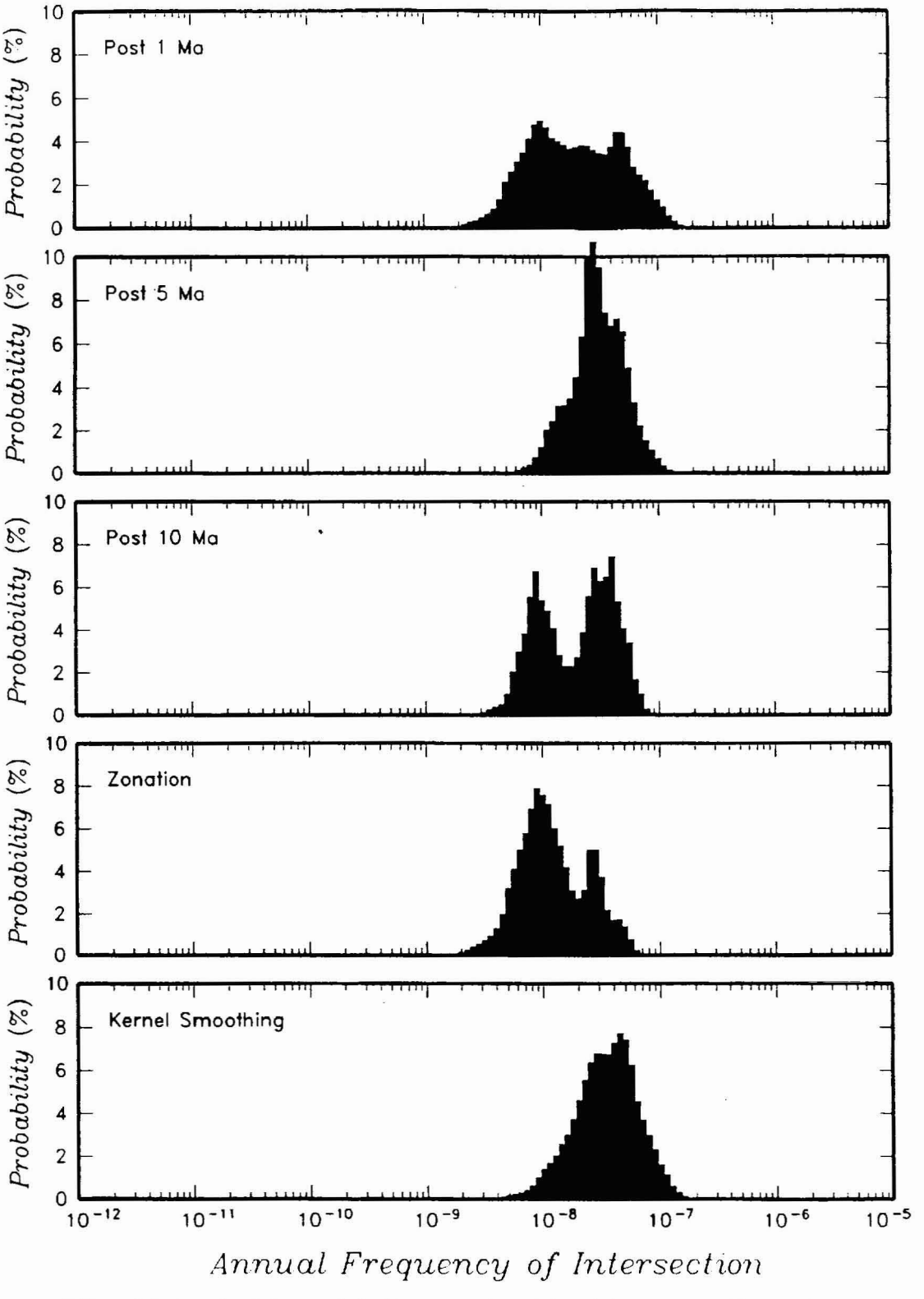

Figure 4-30 Effect of choice of and time period of interest and spatial model on computed hazard distribution for William Hackett's PVHA model.

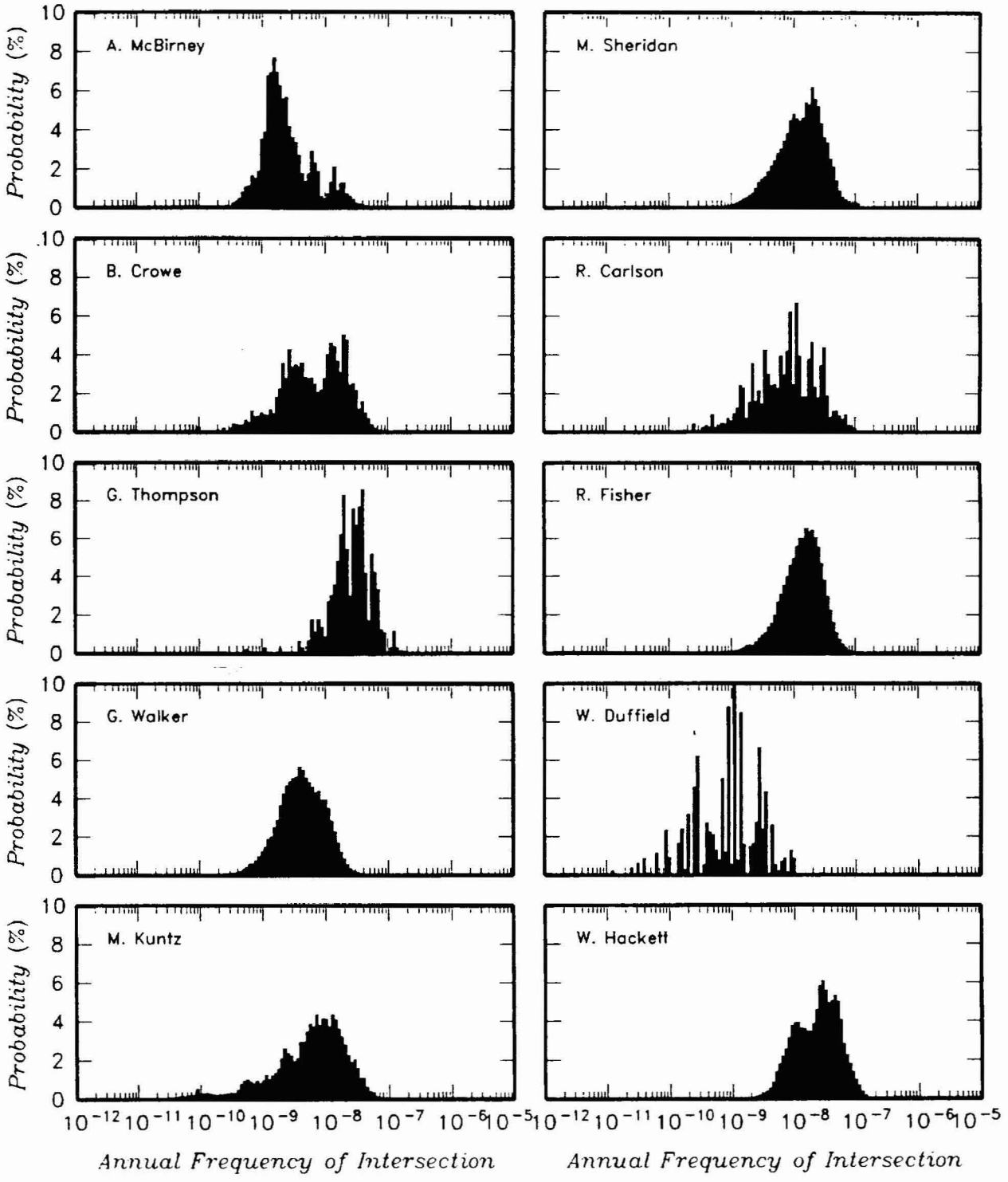

Figure 4-31 Comparison of individual expert distributions for frequency of intersection.

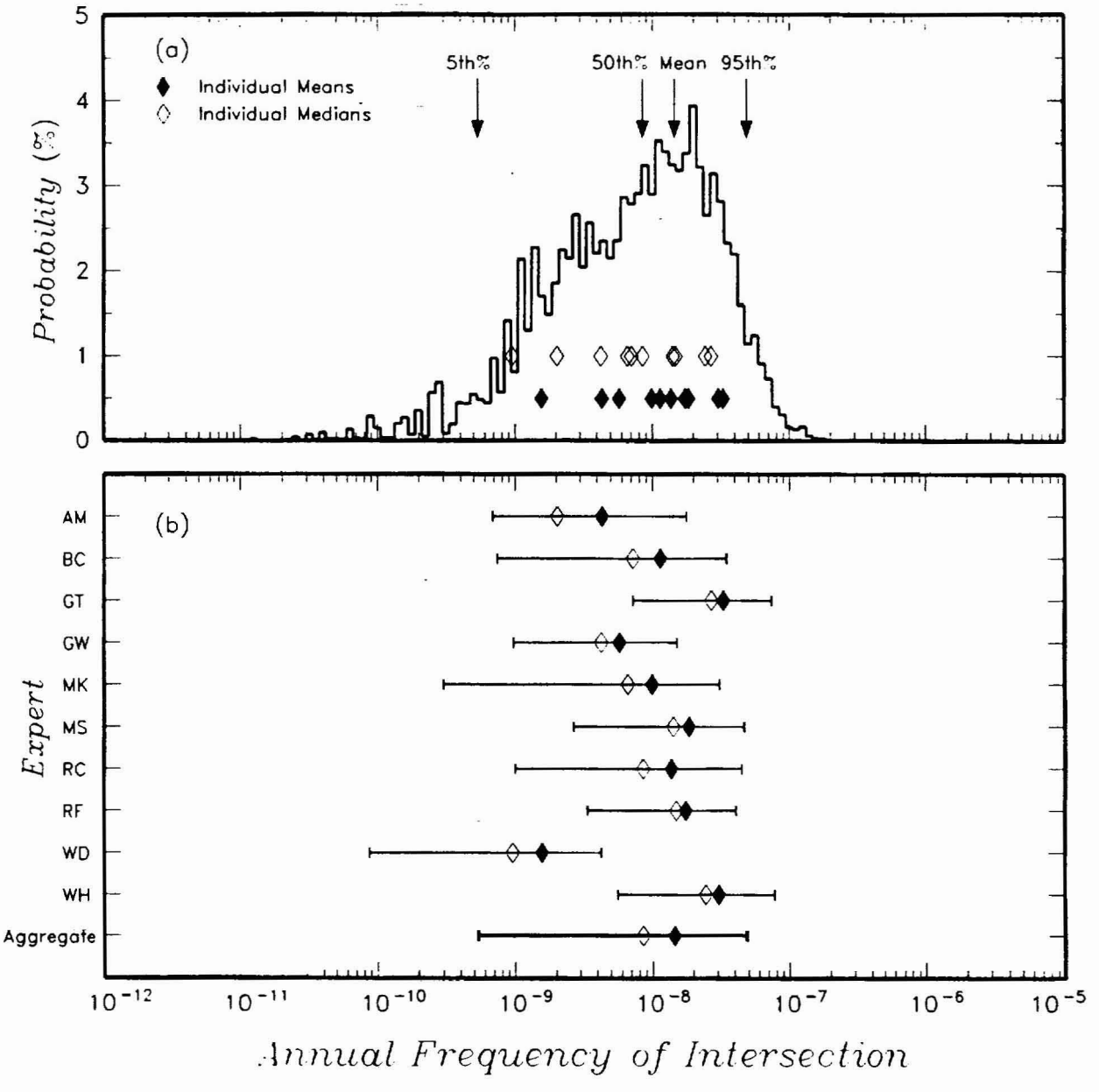

Figure 4-32 Aggregate results for frequency of intersecting the Yucca Mountain repository foot print by a volcanic event. (a) Aggregate distribution for frequency of intersection. (b) Individual and aggregate means, medians, and 90-percent confidence intervals (horizontal bars).

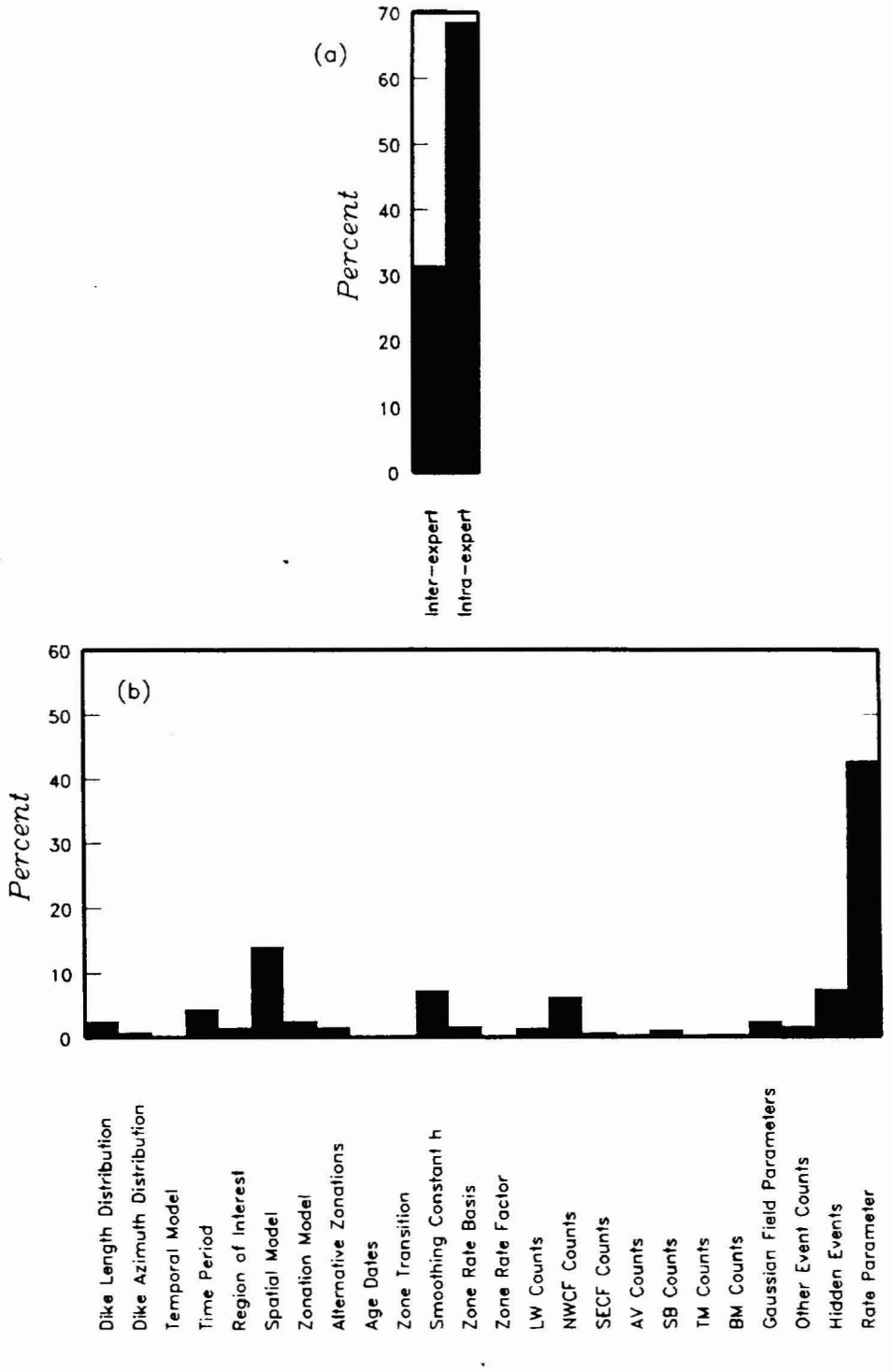

Figure 4-33 Relative contribution of uncertainty in various components of the aggregate PVHA model to the total variance in annual frequency of intersection. (a) Comparison of inter-expert and intra-expert components. (b) Breakdown of intra-expert component of variance.

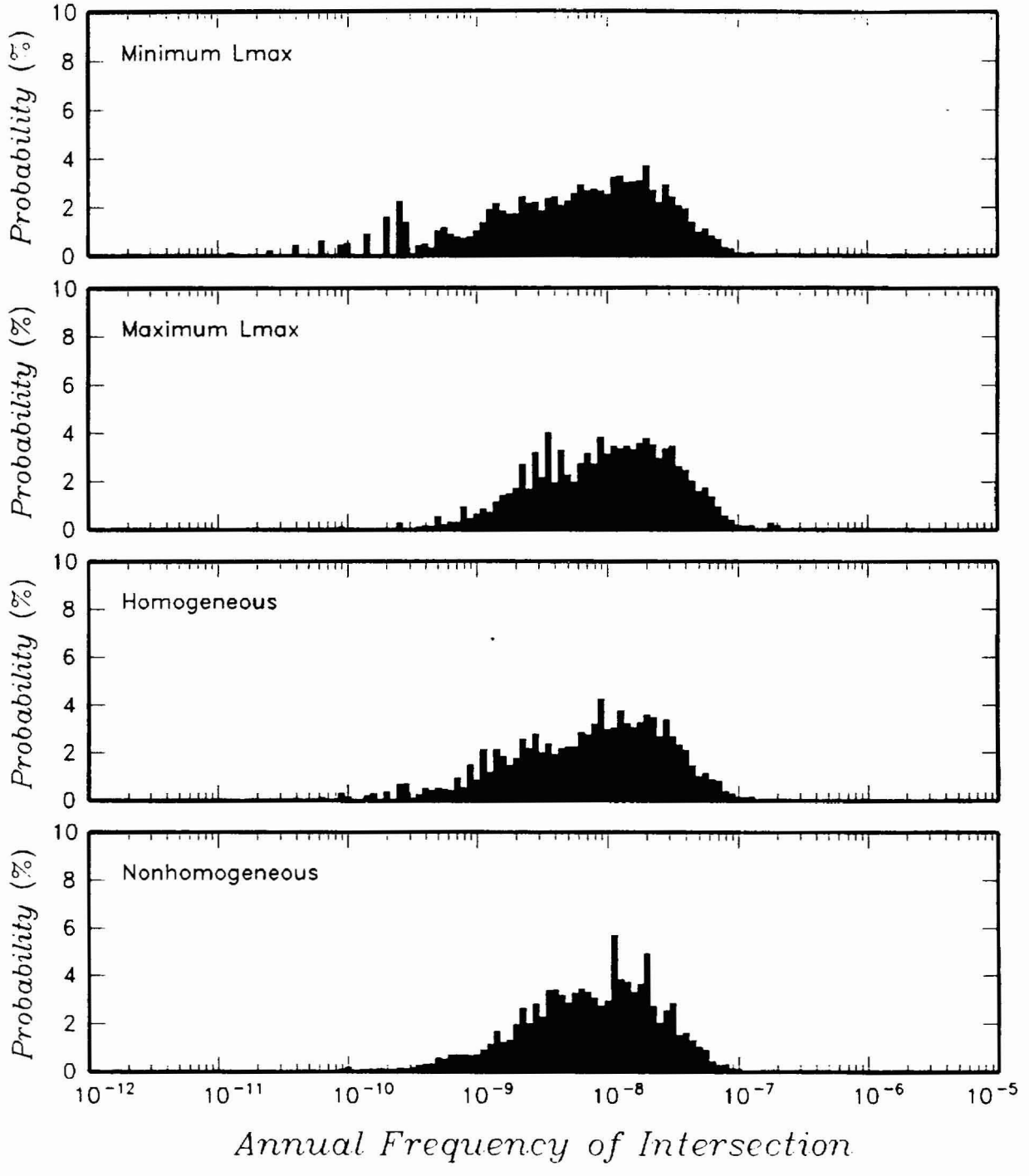

Figure 4-34 Effect of maximum dike length and temporal model on aggregate hazard distribution.

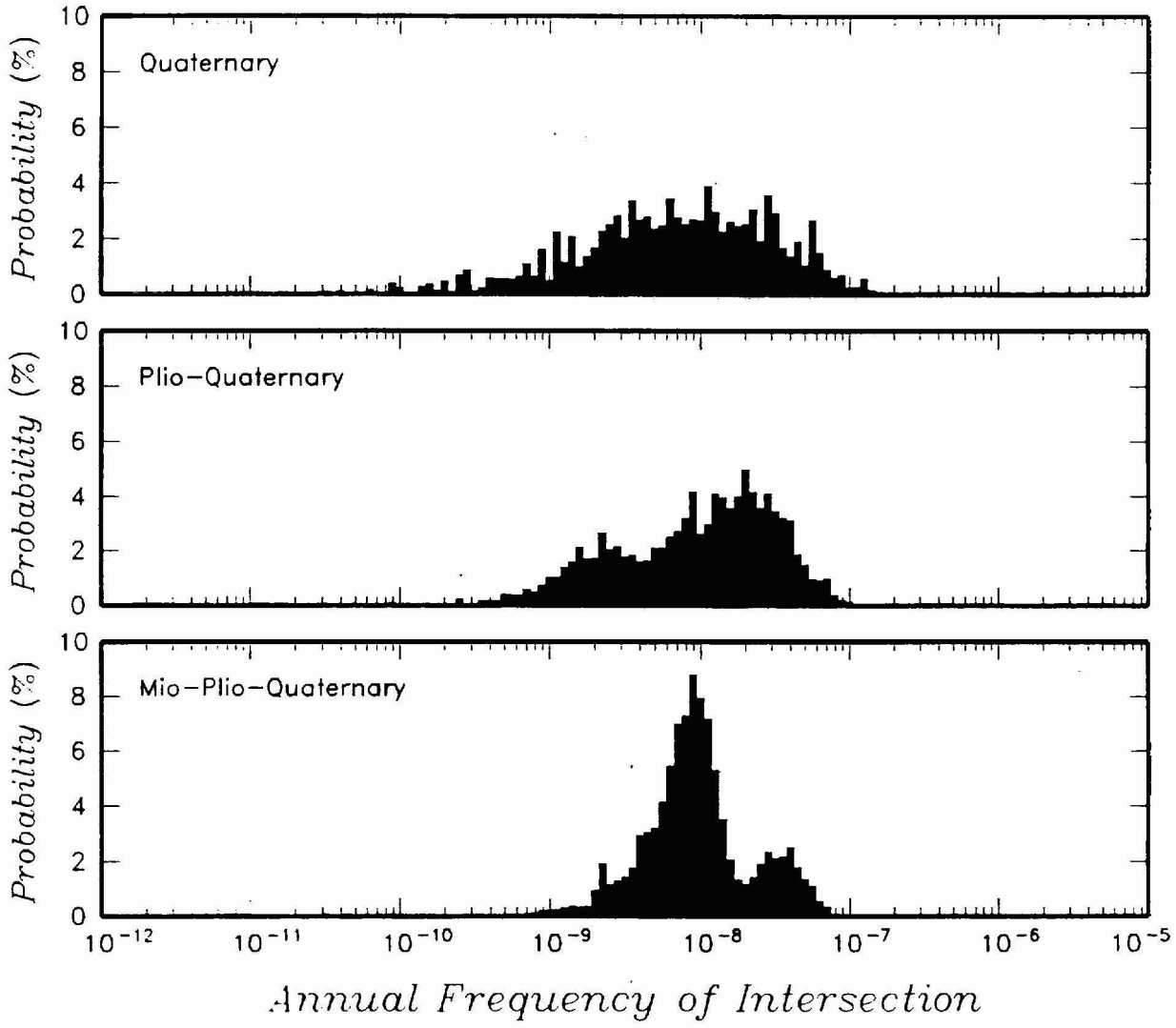

Figure 4-35 Effect of choice of time period on aggregate hazard distribution. Time periods are Quaternary (post 1 to 2 Ma), Plio-Quaternary (post ~5 Ma), and Mio-Plio-Quaternary (post ~10 Ma).

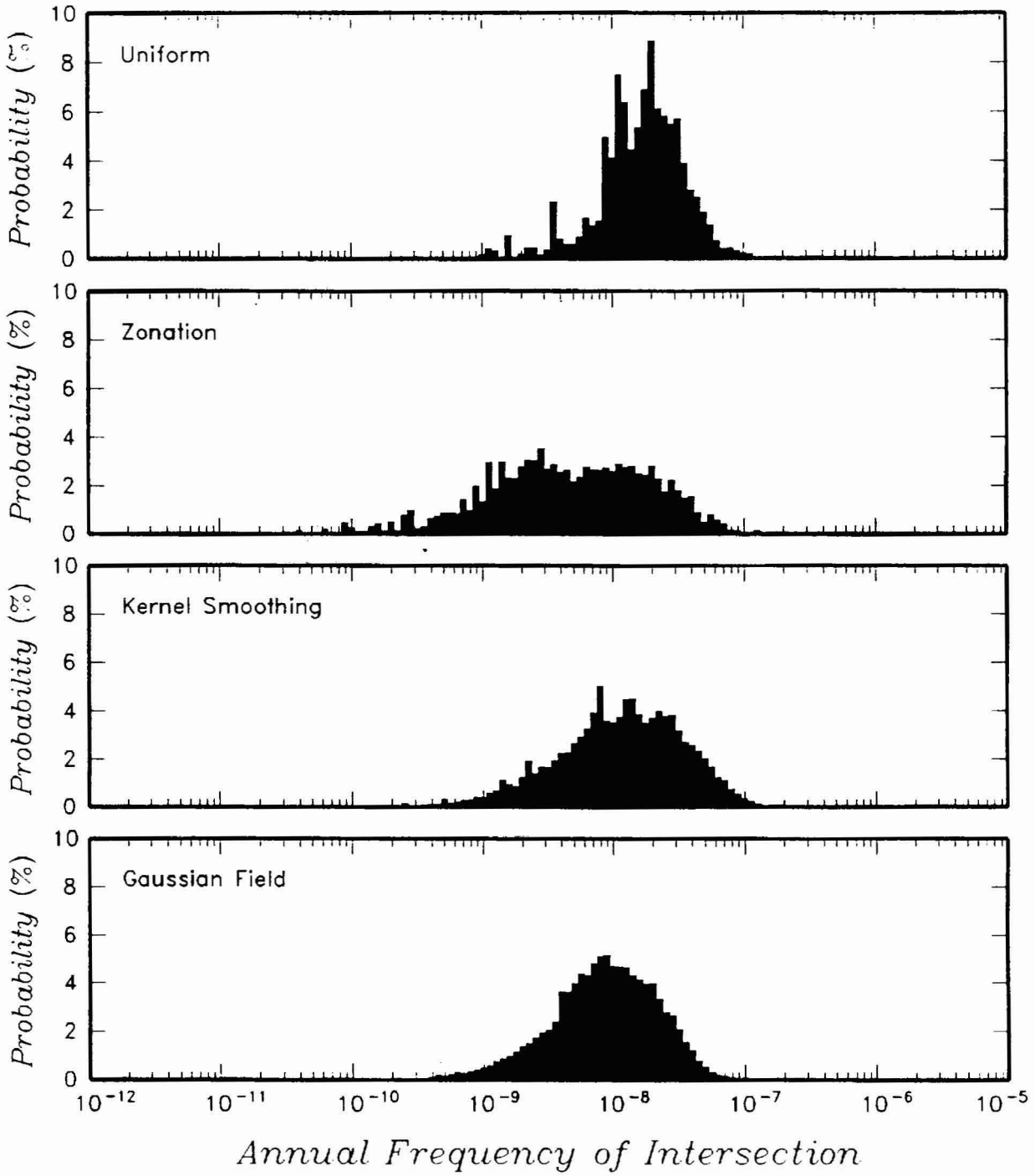

Figure 4-36 Effect of choice of spatial model on aggregate hazard distribution.

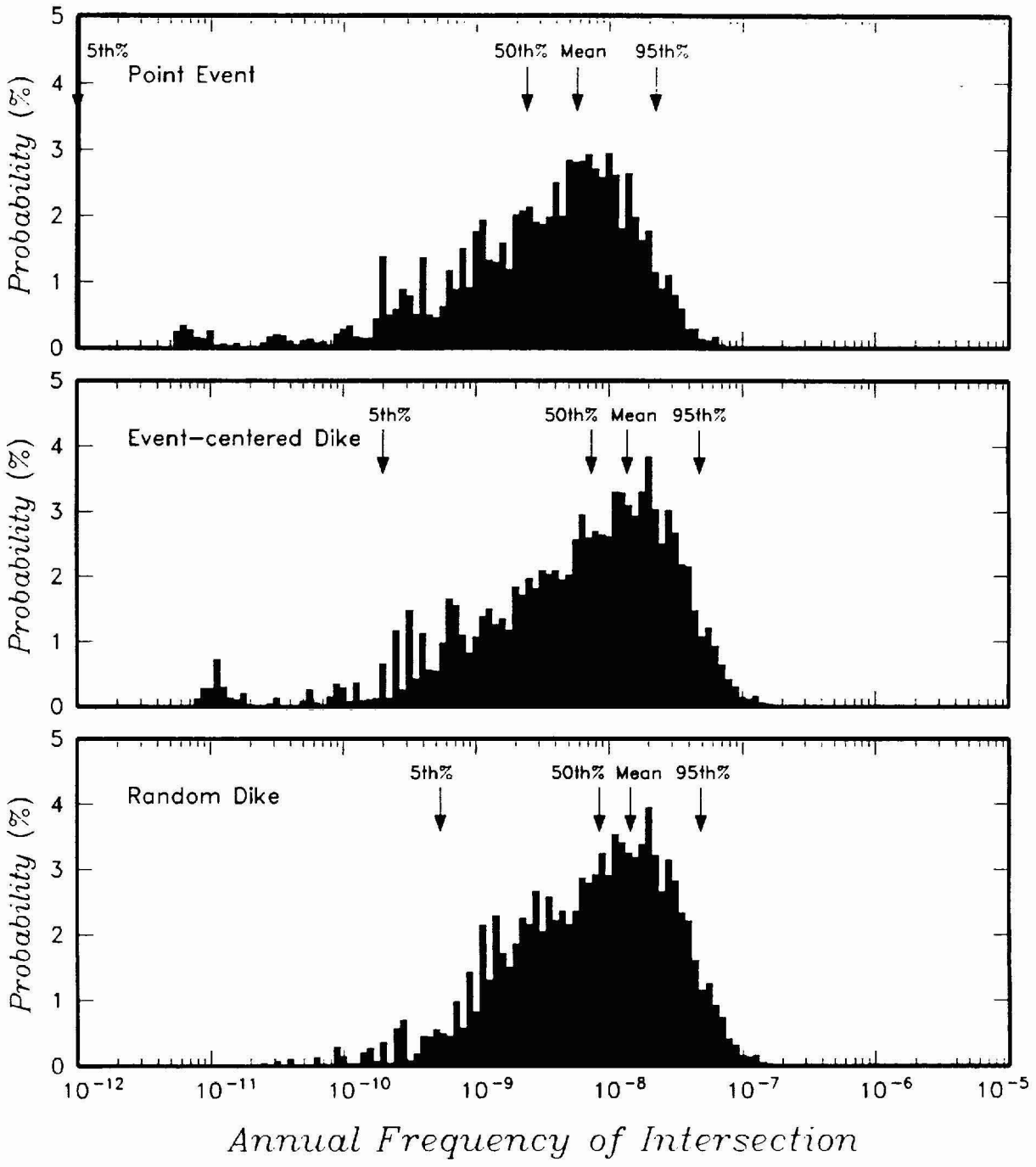

Figure 4-37 Comparison of aggregate distributions for frequency of intersection computed using the three event representations shown on Figure 3-11.

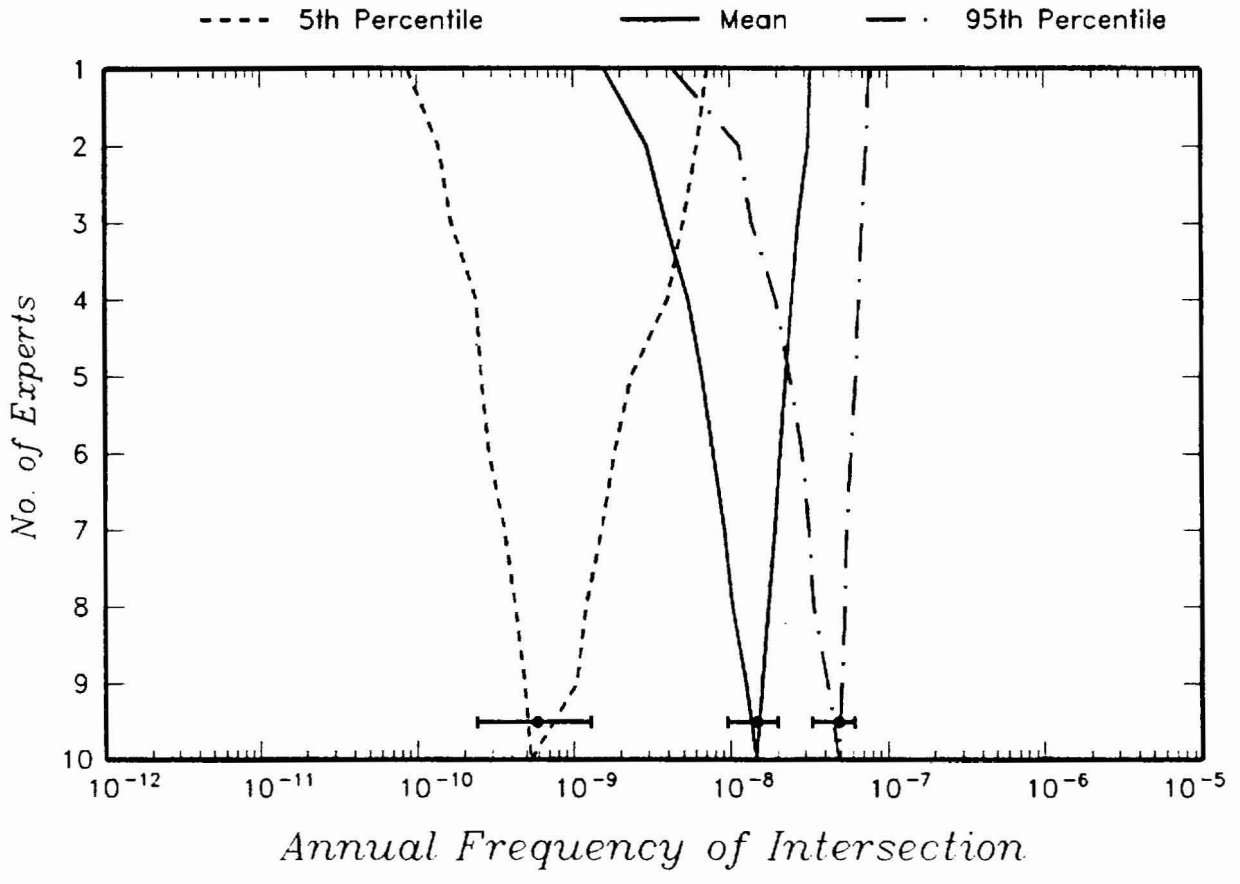

Figure 4-38 Evaluation of the variability in the estimates of the mean and 5th and 95th percentiles of the aggregate hazard distribution. The dashed, solid and dash-dot curves show the limits of the associated statistics considering all possible subsets of varying numbers of experts. The horizontal error bars show the 90-percent confidence intervals and the dots the median values for 1,000 bootstrap simulations of the aggregate distribution.

5. REFERENCES

Bernreuter, D.L., Savy, J.B., Mensing, R.W., and Chen, J.C., 1989, Seismic hazard characterization of 69 nuclear power plant sites east of the Rocky Mountains: U.S. Nuclear Regulatory Commission, NUREG/CR-5250.

Brillinger, D.R., 1982, Some bounds for seismic risk: Bulletin of the Seismological Society of America, v. 72, p. 1403-1410.

Connor, C.B., and Hill, B.E., 1995, Three nonhomogeneous poisson models for the probability of basaltic volcanism: Application to the Yucca Mountain region, Nevada, USA: Journal of Geophysical Research, v. 100, no. B6, p. 10,107-10,125.

Coppersmith, K.J., Perman, R.C., and Youngs, R.R., 1993, Earthquakes and tectonics expert judgement elicitation project: prepared by Geomatrix Consultants for the Electric Power Research Institute, Report TR-102000, project 3055-13.

Coppersmith, K.J., and Youngs, R.R., 1986, Capturing uncertainty in probabilistic seismic hazard assessments within intraplate environments: Proceedings, Third National Conference on Earthquake Engineering, v. 1, p. 301-312.

Coppersmith, K.J., and Youngs, R.R., 1990, Probabilistic seismic-hazard analysis using expert opinion; an example from the Pacific Northwest, *in* E.L. Krinitzsky and D.B. Slemmons (eds.), Neotectonics in Earthquake Evaluation, Boulder, Colorado: Geological Society of America Reviews in Engineering Geology, v. 8.

Cornell, C.A., 1968, Engineering seismic risk analysis: Bulletin of the Seismological Society of America, v. 58, p. 1583-1606.

Cornell, C.A., 1971, Probabilistic analysis of damage to structures under seismic loads *in* Howells, D.A., Haigh, I.P., and Taylor, C., (eds.), Dynamic Waves in Civil Engineering: John Wiley, London.

Crow, L.H., 1974, Reliability analysis of complex repairable systems: *in* Proschan, F. and Serfling, R.J. (eds.), Reliability and Biometry: SIAM, Philadelphia, Penn, p. 392-410.

Crow, L.H., 1982, Confidence interval procedures for the Weibull process with applications for reliability growth: Technometrics, v. 24, p, 67-72.

Crowe, B.M., Johnson, M.E., and Beckman, R.J., 1982, Calculation of the probability of volcanic disruption of a high-level radioactive waste repository within southern Nevada, USA: Radioactive Waste Management, v. 3, p. 167-190.

Crowe, B.M., Perry, F.V., Geissman, J., McFadden, L., Wells, S., Murrell, M., Poths, J., Valentine, G.A., Bowker, L., and Finnegan, K., 1995, Status of volcanism studies for the Yucca Mountain site characterization projects: Los Alamos National Laboratory Report LA-12908-MS, issued March, 1995.

Crowe, B.M., Picard, M., Valentine, G., and Perry, F.V., 1992, Recurrence models of volcanic events; applications to volcanic risk assessment: Proceedings, Third International Conference, High Level Radioactive Waste Management, Las Vegas, Nevada, April 12-16, v. 2, p. 2344-2355.

Department of Energy, U.S., 1995, Principles and guidelines for formal use of expert judgment by the Yucca Mountain site characterization project: Office of Civilian Radioactive Waste Management,Yucca Mountain Site Characterization Office, May, 10 p.

DeWispelare, A.R., Herren, L.T., Miklas, M.P., and Clemen, R.T., 1993, Expert elicitation of future climate in the Yucca Mountain vicinity—Iterative Performance Assessment Phase 2.5: Center for Nuclear Waste Regulatory Analyses, CNWRA 93-016, San Antonio, Texas, August.

Electric Power Research Institute, 1986, Seismic hazard methodology for the central and eastern United States: EPRI NP-4726, project 101-21.

Geomatrix Consultants, Inc., 1988, Seismic hazards assessment for WNP-3, Satsop, Washington: prepared for the Washington Public Power Supply System, contract C-20453.

Ho, C.-H., 1991, Time trend analysis of basaltic volcanism for the Yucca Mountain site: Journal of Volcanology and Geothermal Research, v. 46, p. 61-72.

Ho, C.-H., 1992, Risk assessment for the Yucca Mountain high-level nuclear waste repository site: Estimation of volcanic disruption: Mathematical Geology, v. 24, no. 4, p. 347-364.

Ho, C.-H., Smith, E.I., Feuerbach, D.L., and Naumann, T.R., 1991, Eruptive probability calculations for the Yucca Mountain site, USA: statistical estimation of recurrence rates: Bulletin of Volcanology, v. 54, p. 50-56.

Keefer, D.L., and Bodily, S.E., 1983, Three-point approximations for continuous random variables: Management Science, v. 29, p. 595-609.

Kotra, J.P., Lee, M.P., Eisenberg, N.A., and DeWispelare, A.R., 1996, Branch technical position on the use of expert elicitation in the High-Level Radioactive Waste Program: U.S. Nuclear Regulatory Commission, NUREG-Public Comment Draft, February, 44 p.

Kulkarni, R.B., Youngs, R.R., and Coppersmith, K.J., 1984, Assessment of confidence intervals for results of seismic hazard analysis: Proceedings of the Eighth World Conference on Earthquake Engineering, San Francisco, California, v. 1, pp. 263-270.

Meyer, M.A. and Booker, J.M., 1991, Eliciting and Analyzing Expert Judgment: A Practical Guide: Academic Press Inc., San Diego, CA 92101, 452 p.

National Research Council, 1988, Probabilistic Seismic Hazard Analysis: National Academy Press, Washington D.C., 97 p.

Nuclear Regulatory Commission, 1990, Severe accident risks: an assessment for five U.S. nuclear power plants: U.S. Nuclear Regulatory Commission, NUREG-1150.

Savy, J.B., Bernreuter, D.L., Chen, J.C., Davis, B.C., Ueng, J., and Short, C., 1992, Seismic hazard characterization of the DOE new production reactor sites: NPR92-147JBS, rev. A, draft report, March 31.

Senior Seismic Hazard Analysis Committee (SSHAC), 1995, Recommendations for probabilistic seismic hazard analysis: guidance on uncertainty and use of experts: U.S. Nuclear Regulatory Commission NUREG/CR-6372 and LLNL UCRL-ID-122160, sponsored by U.S. Department of Energy, U.S. Nuclear Regulatory Commission, and Electric Power Research Institute, 170 p.

Sheridan, M.F., 1992, A Monte Carlo technique to estimate the probability of volcanic dikes: Proceedings, High Level Radioactive Waste Management, v. 2, p. 2033-2038.

Silverman, B.W., 1986, Density Estimation for Statistics and Data Analysis, Monographs on Statistics and Applied Probability 26: Chapman and Hall, New York.

Trauth, K.M., Rechard, R.P., and Hora, S.C., 1991, Expert judgement as input to waste isolation pilot plant performance assessment calculations: probability distributions of significant system parameters: Mixed Waste, Proceedings of the First International Symposium, Baltimore, Maryland, August 26-29.

Weichert, D.H., 1980, Estimation of the earthquake recurrence parameters for unequal observation periods for different magnitudes: Bulletin of the Seismological Society of America, v. 70, p. 1337-1346.

APPENDIX A

BIOGRAPHIES
MEMBERS OF THE EXPERT PANEL
PROBABILISTIC VOLCANIC HAZARD ANALYSIS PROJECT